Realia et Realia naturalia

ANNA ŠUGAI

Creation of structural defects under superhigh-dense irradiation of wide-gap metal oxides

TARTU ÜLIKOOL · UNIVERSITAS TARTUENSIS · 1632

ANNA ŠUGAI

Creation of structural defects under superhigh-dense irradiation of wide-gap metal oxides

This study was carried out at the Institute of Physics, University of Tartu, Estonia.

The dissertation was admitted on June 21, 2013, in partial fulfillment of the requirements for the degree of Doctor of Philosophy in physics (solid state physics) and allowed for defence by the Scientific Council of the Institute of Physics, University of Tartu.

Supervisor: Prof. Aleksandr Lushchik, Institute of Physics, University of Tartu

Opponent: Dr. Anatoli Popov, Institute of Solid State Physics, Riga, Latvia

Commencement: At the Senati Hall of University of Tartu, Ülikooli 18, on
                September 11, 2013 at 15.15.

Publication of the thesis was supported by Graduate School on Functional Materials and Technologies (GSFMT), University of Tartu.

CONTENTS

LIST OF PUBLICATIONS

List of the original papers included in this thesis

[I]   A. Lushchik, Ch. Lushchik, V. Nagirnyi, S. Pazylbek, O. Sidletskiy, K. Schwartz, E. Shablonin, **A. Shugai**, E. Vasil'chenko, "On the mechanisms of radiation damage and prospects of their suppression in complex metal oxides," *Physica Status Solidi* B **250** (2), 261−270 (2013)

[II] A. Lushchik, T. Kärner, Ch. Lushchik, K. Schwartz, F. Savikhin, E. Shablonin, **A. Shugai**, E. Vasil'chenko, "Electronic excitations and defect creation in wide-gap MgO and $Lu_3Al_5O_{12}$ crystals irradiated with swift heavy ions," *Nuclear Instruments and Methods in Physics Research* B **286**, 200−208 (2012)

[III] A. Lushchik, Ch. Lushchik, K. Schwartz, F. Savikhin, E. Shablonin, **A. Shugai**, E. Vasil'chenko, "Creation and clustering of Frenkel defects at high density of electronic excitations in wide-gap materials," *Nuclear Instruments and Methods in Physics Research* B **277**, 40−44 (2012)

[IV] A. Lushchik, Ch. Lushchik, T. Kärner, P. Liblik, V. Nagirnyi, E. Shablonin, **A. Shugai**, E. Vasil'chenko, "Franck-Hertz effect in cathodo- and photoluminescence of wide-gap materials", Radiation Measurements **45** (3−6), 268−272 (2010)

[V]   A. Lushchik, Ch. Lushchik, K. Schwartz, E. Vasil'chenko, T. Kärner, I. Kudryavtseva, V. Isakhanyan, **A. Shugai**, "Stabilization and annealing of interstitials formed by radiation in binary metal oxides and fluorides," *Nuclear Instruments and Methods in Physics Research* B **266** (12–13), 2868−2871 (2008)

The author's contribution to the publications:

The papers that form the basis of the thesis are the result of collective work with important contributions by all the coauthors. The author has given an essential input to all the publications; her contribution to the papers can be described as follows:

Publication I: The main author of the Sections "Radiation effects in $Lu_3Al_5O_{12}$ and $Lu_3Al_5O_{12}:Ce^{3+}$" and "Radiation effects in Gd_2SiO_5"

Publication II: The main author of the Section "Radiation effects in lutetium garnet"

Publication III: Obtaining, processing and analysis of experimental data related to Al_2O_3. Participation in the preparation of figures, writing of the manuscript

Publication IV: Participation in the elaboration of the general concept on the solid-state analogue of the Franck-Hertz effect in metal oxides

Publication V: Obtaining, processing and analysis of experimental data related to Al_2O_3. Participation in the preparation of figures

Other publications:

[VI]   A. Lushchik, V. Nagirnyi, K. Schwartz, E. Shablonin, **A. Shugai**, "Electronic excitations and defect creation in $Lu_3Al_5O_{12}$ crystals irradiated with swift heavy ions," in *HASYLAB Activity Report 2011,* DESY, Hamburg, Germany, two pages in the online version

[VII] A. Lushchik, S. Dolgov, I. Kudryavtseva, T. Kärner, F. Savikhin, E. Vasil'chenko, E. Shablonin, **A. Shugai**, "Attenuation of radiation damage in dielectric and composite materials of interest for a fusion reactor," in *Fusion Yearbook Association Euratom-Tekes, Annual Report 2009*, VTT Publications 7389, Helsinki, Finland, pp. 69–72 (2010)

[VIII] **A. Shugai** "Creation processes of radiation defects under conditions of high density of electronic excitations in Al_2O_3 and SiO_2 crystals," *Master thesis*, Tartu University, 2008

List of conferences:

[IX]   A. Lushchik, Ch. Lushchik, I. Kudryavtseva, S. Pazylbek, E. Shablonin, **A. Shugai**, E. Vasil'chenko, "Luminescence and radiation defects creation in heavy-ion-containing metal oxides," *17th International Conference on Radiation Effects in Insulators (REI-2013),* Helsinki, Finland, June 30–July 05, 2013 (poster).

[X]   A. Lushchik, Ch. Lushchik, V. Nagirnyi, S. Pazylbek, O. Sidletskiy, K. Schwartz, E. Shablonin, **A. Shugai**, E. Vasil'chenko, "On the non-impact mechanisms of radiation damage and prospects of their suppression in complex metal oxides," *International Conference on Defects in Insulating Materials (ICDIM 2012),* Santa Fe, USA, June 24–29, 2012, p. 35 (oral talk).

[XI]   **A. Shugai**, A. Lushchik, M. Nikl, F. Savikhin, K. Schwartz, E.Vasil'chenko, "Luminescent protection against defect creation in $Lu_2Al_5O_{12}$:Ce," *Intern Conf. Functional Materials and Nanotechnologies (FM&NT-2012),* Riga, Latvia, April 17–20, 2012, p.89 (oral talk).

[XII] **A. Shugai**, "Luminescent protection against defect creation in $Lu_3Al_5O_{12}$:Ce", *TÜ ja TTÜ doktorikooli "Funktsionaalsed materjalid ja tehnoloogiad" kolmas teaduskonverents*, Tartu, Estonia, February 29–March 1, 2012 (poster).

[XIII] A. Lushchik, Ch. Lushchik, K. Schwartz, F. Savikhin, E. Shablonin, **A. Shugai**, E. Vasil'chenko, "Contribution of electronic excitations to defect creation in wide-gap metal oxides irradiated with swift heavy ions or fast electrons," *16th International Conference on Radiation Effects in Insulators (REI-2011),* Beijing, China, August 14–19, 2011, I-1, Abstr. p. 34 (invited lecture).

[XIV] A. Lushchik, Ch. Lushchik, K. Schwartz, F. Savikhin, E. Shablonin, **A. Shugai**, E. Vasil'chenko, "Creation and clustering of Frenkel defects at high density of electronic excitations in wide-gap materials," *EMRS 2011 Spring Meeting, Symposium L "Basic research on ionic-covalent materials for nuclear applications",* Nice, France, May 9−13, 2011 L3-5 (oral talk).

[XV] I. Kudryavtseva, A. Lushchik, A. Maaroos, Z. Salikhoja, **A. Shugai**, "Contribution of electron-hole processes to luminescence of $CaSO_4$ doped with RE^{3+} ions," *Intern Conf. Functional Materials and Nanotechnologies (FM&NT-2011),* Riga, Latvia, April 5−8, 2011, PO-21, p. 111 (poster).

[XVI] **A. Shugai**, A. Lushchik, M. Nikl, F. Savikhin, K. Schwartz, E. Vasil'chenko, "Radiation damage induced by swift heavy ions in $Lu_2Al_5O_{12}$ crystals," *Intern Conf. Functional Materials and Nanotechnologies (FM&NT-2011),* Riga, Latvia, April 5−8, 2011, OR-2, p. 40 (oral talk).

[XVII] **A. Shugai**, "Radiation damage induced by swift heavy ions in $Lu_3Al_5O_{12}$ crystals," *TÜ ja TTÜ doktorikooli "Funktsionaalsed materjalid ja tehnoloogiad" teine teaduskonverents*, Tallinn, Estonia, March 3–4, 2011 (poster).

[XVIII] **A. Shugai**, "Creation processes of Frenkel defects in $Lu_3Al_5O_{12}$ single crystals," *TÜ ja TTÜ doktorikooli "Funktsionaalsed materjalid ja tehnoloogiad" esimene teaduskonverents*, Tartu, Estonia, February 25–26, 2010 (poster).

[XIX] A. Lushchik, Ch. Lushchik, T. Kärner, P. Liblik, V. Nagirnyi, E. Shablonin, **A. Shugai**, E. Vasil'chenko, "Franck-Hertz effect in cathodo- and photoluminescence of wide-gap materials," *7th International Conference on Luminescent Detectors and Transformers of Ionizing Radiation,* Krakow, Poland, July 12−17, 2009, Mo-7 (invited lecture).

[XX] A. Lushchik, Ch. Lushchik, V. Isakhanyan, T. Kärner, P. Liblik, A. Maaroos, **A. Shugai**, E. Vasil'chenko, "Contribution of hot electron-hole recombination into radiation damage of wide-gap materials for nuclear energetics and other applications," *International Baltic Sea Region conference "Functional materials and nanotechnologies,"* Riga, April 1−4, 2008 (oral talk).

[XXI] A Lushchik, Ch. Lushchik, K. Schwartz, E. Vasil'chenko, T. Kärner, I. Kudryavtseva, V. Isakhanyan, **A. Shugai**, "Stabilization and annealing of interstitials formed by radiation in binary metal oxides and fluorides," *14th International Conference on Radiation Effects in Insulators (REI-2007),* Caen, France, August 28−September 1, 2007 (oral talk).

LIST OF ABBREVIATIONS

AD   antisite defects
β   heating rate
CL   cathodoluminescence
e   electron
h   hole
e–h   electron-hole
EE   electronic excitations
E_{FD} creation energy of a Frenkel pair
E_g band gap
EPR   electron paramagnetic resonance
FD   Frenkel defects
hν   photon energy
LET   linear energy transfer
OD   optical density
LuAG $Lu_3Al_5O_{12}$ garnet
GSO Gd_2SiO_5 silicate
RIOA   radiation-induced optical absorption
RT   room temperature
TSL   thermally stimulated luminescence
SHI   swift heavy ions
SR   synchrotron radiation
T_{melt} melting temperature
UV, VUV   ultraviolet, vacuum ultraviolet
v_a, v_c anion vacancy, cation vacancy
WGM   wide-gap material

I. INTRODUCTION

Insufficient radiation resistance is a serious limitation for wide-gap materials (WGM, $E_g = 5{-}15$ eV) possessing other necessary properties to be used as effective fast scintillation detectors and selective dosimeters for medical and industrial purposes, laser hosts and materials for optical components, spectral transformers for environmental-benign (mercury-free) fluorescence lamps and displays, etc. It is assumed that no success in future industrial thermonuclear (fusion) reactors can be achieved without a significant enhancement of the radiation resistance of construction and diagnostic materials (including different dielectric materials).

The contribution of various mechanisms of defect creation to radiation damage depends on the type of solids. In metals and alloys, radiation damage is mainly caused by the knock-out (impact) mechanism connected with elastic collisions of high-energy incident particles (neutrons, light and heavy ions) with the atoms of a crystal, providing their displacement from regular lattice sites and the formation of vacancies and interstitials − the so-called Frenkel defects (FD) as well as extended (dislocations), 2D and 3D nanosize defects (see, e.g. [1, 2]). Irradiation of metals and alloys leads to an especially efficient accumulation of vacancy-interstitial pairs with significant spatial interdefect separation. The formation energy of an interstitial in a metal bulk significantly exceeds the energy needed for the creation of a Schottky defect − replacement of an atom from a regular lattice site in the interior to the surface. So, vacancies are mainly formed in the bulk of an irradiated metal, while interstitials are accumulated in intergranular regions. In recent years, particular emphasis has been laid on the dependence of the efficiency of radiation damage on the grain size (in a nanoscale) of complex metal alloys [3].

In a number of wide-gap dielectrics − WGM, the rapid impact mechanism of FD creation plays a critical role as well [4]. Among these, WGM with a high resistance against low-dense radiation (e.g, γ-rays), there are binary and complex two- or trivalent metal oxides (MgO, Al_2O_3, $MgAl_2O_4$, $Y_3Al_5O_{12}$, etc) where the threshold energy for the creation of an FD pair is high, $E_{FD} \gg E_g$ (see, e.g. [4]). However, the value of E_{FD} is about twice lower (but still $E_{FD} > E_g$) for another, slower adiabatic mechanism of FD creation connected with the excitation and ionisation of an electron subsystem.

On the other hand, the inequality $E_{FD} < E_g$ is valid for many other WGM. In particular, in a number of alkali halides with anions and cations, close in size, and a loose packing of ions, FD are efficiently created at the decay of self-trapping excitons or at the recombination of relaxed (cold) conduction electrons (*e*) with the holes (*h*) rapidly undergoing self−trapping [5−7]. These excitonic and *e*−*h* mechanisms were revealed by measuring the creation spectra of FD (F−H pairs) by vacuum ultraviolet (VUV) radiation at 4.2 K in many alkali halides. However, even among them there exist some crystals with a close-packed lattice (NaCl, NaBr and NaI with large-radius anions) where the creation effi-

ciency of long-lived (stable) F–H pairs via the decay of excitons or the recombination of e with self-trapped h (V_K centers) at helium temperatures is low. Recently, it was shown, that the irradiation of NaCl ($E_g = 8.9$ eV) by the 15–16-eV photons at 10 K creates stable F–H due to hot e–h recombination [8, 9]. The main criteria ("energetic, time and orientation") of the efficient decay of selectively formed electronic excitations (EE) into FD in ionic crystals were considered in [6, 10].

After engineering of the Mesyats-Koval'chuk-type generator of powerful electron pulses (GIN-600: 3 ns, 10^2–10^4 A/cm^2), the following phenomena were discovered in WGM [11–13]: (i) a fast (<< 1 ns) and temperature-independent intraband luminescence related to radiative transitions of hot electrons/holes between the levels of the conduction/valence band; (ii) a fast (< 1 ps) coherent migration of hot carriers; and (iii) a cracking and brittle destruction of single crystals at a high current density (> 10^2–10^3 A/cm^2). The use of single powerful electron pulses causes the irradiation of large areas (~5 × 5 mm^2) of a single crystal surface resulting in hampering of the motion of radiation-induced dislocations toward the surface and a cracking of the crystal. Although the volume density of the EE induced by such electron pulses is relatively low (intermediate between that for protons and α-particles), the large excited area allows detecting very weak intrinsic emissions, for instance, intraband luminescence in alkali halides. The novel creation mechanisms of nano- and macro-size defects are especially efficient under irradiation of WGM with swift heavy ions (SHI: ^{197}Au, ^{238}U, ~GeV), which spend more than 99% of their energy on ionisation losses providing an extremely high density of EE (LET > 20 keV/nm) within cylindrical ion tracks [14–16].

It is worth noting that according to theoretical predictions, a new kind of intrinsic localized mode with a large amplitude and frequency above the top of the acoustic phonon spectrum may exist under the dense excitation of a crystal lattice predisposed to anharmonic interactions [17–20]. Such unusual excitations, also referred to as discrete breathers or discrete solitons, are expected to be especially strong in the WGM built up of ions with very different masses – the frequency of discrete breathers can fall in a gap between acoustic and optical vibration branches.

In wide-gap complex metal oxides with $E_{FD} > E_g$ and many atoms per unit cell (e.g., pure and rare-earth-doped $Y_3Al_5O_{12}$, $Lu_3Al_5O_{12}$, Y_2SiO_5, Gd_2SiO_5), the contribution of all the three defect creation mechanisms is expected at the irradiation with SHI providing a partial overlapping of cylindrical ion tracks (at a fluence of 10^{12} ions/cm^2, the average distance between tracks is ~10 nm). On the other hand, the third mechanism of radiation damage is supposed to be inefficient in the binary pure MgO single crystals with $E_{FD} > E_g$ and close masses of anions and cations.

The general goal of the present study was to experimentally reveal the peculiarities of EE, and particularly, of the processes of the creation and thermal annealing of long-lived (stable) radiation damage – Frenkel defects and their asso-

ciations as well as extended and 3D nanosize defects – under irradiation of binary and complex metal oxides with swift heavy ions (~GeV, ^{197}Au, ^{238}U) that cause a superhigh excitation density (LET > 20 keV/nm) within cylindrical ion tracks. In the investigated single crystals, $E_{FD} > E_g$ and a unit cell contains many atoms (number in brackets): α-Al$_2$O$_3$ (10), Lu$_3$Al$_5$O$_{12}$ (160), Gd$_2$SiO$_5$ (32). A comparative spectroscopic study of virgin and SHI-irradiated crystals (both, nominally pure and cerium-doped) was performed using 4–40-eV photons, x-rays (~50 keV) and electrons (4–20 keV; 300 keV). It is worth noting that the used synchrotron radiation (SR, 4–40 eV) and a steady electron beam (4–20 keV) produce EE in a thin layer of the sample, while ns-electron pulses and x-rays excite luminescence in the bulk of single crystals. So, electron pulses can be used for the analysis of the changes in optical characteristics in ~100 μm layer (i.e. crystal bulk) caused by previous irradiation with SHI (the range of incident 300-keV electrons and ~GeV-SHI is sufficiently close).

Special attention was also paid to the prospects of the influence of certain heavy luminescent impurity ions on the efficiency of FD creation via hot e–h recombination and to experimental manifestations of the theoretically predicted creation mechanism of 3D nanosize defects – rearrangement of many host atoms at the collapse of discrete breathers (solitons) [20]. For application reasons, LuAG and GSO contain luminescent heavy rare-earth ions. So, it was important to reveal the dependence of the impurity emission on the concentration of impurity luminescence centers as well as to analyze the contribution of luminescence centers involving two or even more heavy impurity ions (especially, if one of them substitutes for a light matrix ion) on the efficiency of radiation damage in metal oxides.

This thesis is based on the experimental results presented in five original papers [I–V] included in the thesis. Most of the experimental results have been obtained in the Laboratory of Physics of Ionic Crystals at the Institute of Physics, University of Tartu as well as using synchrotron-radiation facility – SUPERLUMI station, HASYLAB at DESY, Germany.

2. EXPERIMENTAL

2.1. Experimental methods and equipment

A comparative study of virgin and irradiated (with low or superhigh excitation density) metal oxide crystals has been performed using SR of 4–40-eV, x-rays, steady and pulsed electron beam, and the methods of optical and thermoactivation spectroscopy in a wide temperature region (6–1425 K).

Particular attention has been given to radiation effects under superhigh density of EE in cylindrical tracks of SHI. Our crystals were irradiated at the UNILAC linear accelerator of the GSI in Darmstadt (see [15, 16] for details). The flux of the 3×10^8 ions s^{-1} cm^{-2} for [197]Au and [238]U heavy ions with the energy of ~2.5 GeV and extremely high energy losses (LET~ 24 keV/nm) was used. To prevent the heating and charging of the samples, irradiation was performed by short pulses: 5 Hz, 50 μs – for low fluences of up to 10^{10} ions/cm^2; and 50 Hz, 5 ms – for higher fluences. Objects were covered with a 5-μm aluminum folium (which reduces SHI energy down to 2.35 GeV) in order to prevent the falling out of the sample. Irradiation with SHI was performed along the growing axis of the crystal.

Table 1. Used bombarding ions and their range in the investigated samples

Object	Bombarding ion	Ion range, μm TRIM code [21]
LuAG	[238]U [197]Au	53.7 65.3
Al$_2$O$_3$	[238]U	60
GSO	[197]Au	69.9
SiO$_2$	[238]U	90

The crystals were hold in vacuum at room temperature (RT) during the procedure. At fluences higher than 2×10^{11} ions/cm^2, there is a partial overlapping of ion tracks further enhancing the density of radiation-induced EE. The thickness of the majority of the objects is approximately 1 mm, only for GSO crystals it was 0.4 mm. As a result, all bombarding particles are stopped in the material bulk. The ion ranges in the investigated WGM calculated via TRIM code [21] are presented in Table 1.

Table 2. Irradiation fluence versus the distance between ion tracks

Fluence, ions/cm^2	3×10^{10}	2×10^{11}	1×10^{12}	5×10^{12}	1×10^{13}
Distance, nm	65.2	22.4	11.3	5.05	3.57

Low-dense irradiation was performed using an x-ray tube with a wolfram anode (55 keV, 15 mA, ~1.5 Gy/s) and a beryllium window. During irradiation the objects were covered with a thin aluminum folium in order to select only high-energy exciting quanta.

Photoluminescence

Photoluminescent measurements were mainly conducted using SR at the SUPERLUMI station of HASYLAB at DESY (Hamburg, Germany) from the DORIS storage ring (see [22] for details). SUPERLUMI experimental setup is optimized for selective excitation in the UV-VUV spectral range and the luminescence analysis from VUV to the near IR range.

The setup includes a primary monochromator for the excitation/reflection and several secondary monochromators for luminescence analysis. The primary normal incidence monochromator has a focal length of 2 m, covers the spectral range of ~3.8 to 40 eV (330–31 nm), and in our experiments the 30 μm wide entrance slit (~0.3 nm instrumental resolution) was used. The working region of the primary monochromator is covered by two gratings: Al-grating (4–20 eV region) and Pt-grating (15–40 eV). Additionally, two filters are used to eliminate excitation by the second orders of Al-grating: a quartz filter for the energies below 6.5 eV and a MgF_2 filter for energies 6–10 eV. Unfortunately, the MgF_2 filter cuts the intensity of excitation, considerably reducing the signal to noise ratio.

The emission spectra were recorded though a 0.3-m Czerny-Turner-type imaging monochromator-spectrograph SpectraPro-308i equipped with a photomultiplier tube R6358P Hamamatsu or liquid nitrogen cooled CCD detector (typical spectral resolution ~1 nm, allows an improved resolution of ~0.1 nm in the red spectral region of~700 nm).

The reflection spectra and the excitation spectra of various emissions were normalized to equal the quantum intensities of SR falling onto the crystal at an incidence angle of 17.5°. The reference signal for normalization was recorded from a sodium salicylate. At the storage ring DORIS the FWHM of SR pulses is 130 ps with a repetition rate of 5 MHz. Such pulsed excitation enables the recording of the spectra for time-integrated luminescence as well as studying the emission detected within several time windows (length $\Delta t = 0.3–198$ ns) correlated with the arrival of SR pulses (delayed δt). The liquid helium flow cryostat allows conducting experiments at 6–300 K.

Optical absorption

The spectra of optical absorption (optical density, OD) were measured before and after irradiation in the spectral region of 1.5–6.5 eV using double-beam spectrometers JASCO V-550 or V-650. The difference between these two spectra is considered the radiation-induced optical absorption (RIOA) of the sample. A high-absorbance spectrometer JASCO V-650 with a double monochromator

and low level of scattered light allows measuring absorbance up to OD = 4. However, above OD = 3.3 instrument's response is nonlinear.

The absorption in the region 4–12 eV was measured using a vacuum monochromator VMR-2 with a linear dispersion of 1.66 nm/mm and variable slit width. The samples were excited using a discharge hydrogen source (incidence angle of 40º to the sample surface normal). To equalize the quantum intensities falling onto the sample, a variable monochromator slit width and the reference signal from sodium salicylate was used.

The annealing of RIOA was performed using a step-by-step regime. After the RIOA spectrum was measured at T_0 = RT, the sample was rapidly heated up to a certain temperature T_1, kept 15 min at this certain temperature and then rapidly cooled down to T_0 ,– and the absorption spectrum was measured once more. After that, the sample was heated up to $T_2 = T_1 + \Delta T$ and the whole procedure was repeated. So, all the RIOA spectra (after every heating) in the region from 1.5 to 8 eV were measured at RT. The preheating up to 800 K was performed using Harshow Model 3500 TLD Reader in the atmosphere of flowing nitrogen. The preheating in the temperature region 800–1425 K takes place in a very dry air atmosphere. A highly pure quartz ampoule with the sample was placed into a furnace preliminarily heated up to the T_i. After insertion of the sample, temperature T_i (measured by Pt-Pt-Rh thermocouple) becomes stabilized in 2 min. The sample was kept at the stabilized T_i for 15 min and then the ampoule with the sample was removed from the furnace and cooled down on a heavy metal piece.

Cathodoluminescence
The spectra of steady cathodoluminescence (CL) were measured with a two-channel setup, which allowed registering luminescence in the region 1.6–11 eV at temperatures 6–420 K. In this setup, excitation is carried out by an electron gun (2–15 keV, typically 300 nA). An electron beam is focused on the surface of an object into a spot of about 0.5 mm^2, and the penetration depth of electrons is ~0.5 and ~1 μm for the energies 5 and 10 keV, respectively. A typical thickness of an object is 0.5–1 mm. The short-wavelength channel (4–11 eV) has a Johnson–Onaka vacuum double monochromator (with a grating for the dispersive element, $\Delta\lambda$ = 0.167 nm/mm) and a R6838 photomultiplier. The channel for longer wavelengths (1.6–6.0 eV) had a double prism monochromator and a photon counter Hamamatsu H6240.

After the electron irradiation was stopped, phosphorescence or thermally stimulated luminescence (TSL, constant heating rate of β = 10 K min^{-1}) of selected energy can be registered in both channels. Additionally, an integrated signal in the region of 1.8–6.0 eV can be registered in one of the channels by an additional outer detector, which is mounted onto the object window of the cryostat.

The spectra of fast emissions were measured using powerful single electron pulses from the Kovalt'chyk-Mesyats type GIN-600 generator (3 ns, the current density 1–180 A cm^{-2}, the maximum energy of 300 keV). The emission from

the sample, placed into a cryostat (80−700 K), was recorded through a double prism monochromator DMR-4 (1.2−5.8 eV) or a single grating vacuum mono-chromator VMR-2 (4−10 eV) by a system consisting of photomultipliers EMI 9863 B/Q and an oscilloscope Tektronix TDS-3032. All necessary corrections have been performed for the spectra of fast emissions. The range for 300-keV does not exceed 170 μm (for LuAG and GSO, having a density of 6.7 g/cm^3).

Thermally stimulated luminescence

The TSL from 5 to 823 K was measured using two different set-ups. The first one, for the spectrally integrated signal or a given emission and temperature region of 6−420 K is already described in the Section "Cathodoluminescence". The high-temperature TSL (300−875 K) was measured at the heating of the previously irradiated samples with a constant rate of $\beta = 2$ K s^{-1} in the atmos-phere of flowing nitrogen, using an Harshow Model 3500 TLD Reader or Sys-tem 310 TLD Reader. It was possible to register a spectrally integrated (1.9−4.1 eV) signal or the TSL selected by optical filters.

2.2. Investigation objects

α-Al$_2$O$_3$

α-Al$_2$O$_3$ has a dense hexagonal close-packed lattice (formed by oxygen ions). Al^{3+} ions are located in 2/3 octahedral cavities (see Fig. 1). Each aluminum ion (Al$^{~3+}$) is surrounded by 6 oxygen atoms, while oxygen ions (O$^{~2-}$) are located inside distorted Al tetrahedrons. An elementary cell can be chosen in the form of a six-edged prism with a =4.75Å and c = 12.97Å. As the structure is slightly deformed, the local symmetry of sites is low − C$_3$ for cations in regular cavities, C$_2$ − for anions. The Al−O bonding type is basically ionic [23].

Figure 1. α-Al$_2$O$_3$ structure [23].

The investigated α-Al_2O_3 or ruby (Al_2O_3:Cr^{3+}, 0.05 w% of Cr_2O_3) single crystals were prepared in Russia by horizontal-oriented crystallization method (zone melting). Growth directions are possible within 60 degrees to the main crystal axis or coincide with the main axis [24].

$Lu_3Al_5O_{12}$ (LuAG)

On the basis of crystallographic properties, LuAG (isostructural to $Y_3Al_5O_{12}$) single crystal has bcc cubic structure with space group O_h^{10} (Ia$\bar{3}$ d). An elementary cell contains 8 formula units or 160 atoms. In the elementary cell, Al^{3+} ions are located in two types of lattice sites with a different oxygen coordination: 16 octahedral (a-site, C_{3i}=S_6) and 24 tetrahedral (d-site, S_4). Lu ions are placed in 24 dodecahedral c-sites. There are 8 nonequivalent a-sites, 6 d-sites and 6 nonequivalent c-sites. Sometimes an Lu^{3+} ion can sit in the Al^{3+} octahedral position, this complex is named as antisite defect (AD, $Lu^{3+}|_{Al}^{3+}$, or $Lu|_{Al}$). As a rule, large-radius impurities (such as Ce^{3+}) replace Lu^{3+} ion in the LuAG lattice. The lattice constant at RT is 12 Å, the distance Al−O in tetrahedrons is 1.76 Å, in octahedrons −1.94 Å, while the distance Lu−O equals 2.37 Å [25, 26]. Each oxygen is a member of two dodecahedra, one octahedron and one tetrahedron.
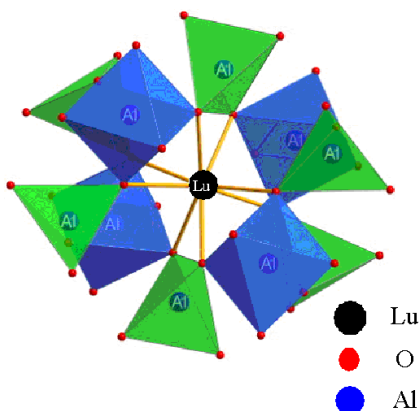
Figure 2. $L_3Al_5O_{12}$ structure [26].

Nominally pure and Ce^{3+}-doped LuAG were grown by the Czochralski method from 5N Lu_2O_3 and 4N Al_2O_3 starting materials in a molybdenum crucible under the reducing atmosphere at CRYTUR, Ltd., Turnov, Czech Republic (see [27−30] for details). In nominally pure LuAG crystals, we estimated the concentration of Ce^{3+} as not more than 30 ppm, while, according to [31], these samples contained about 0.5 at% of antisite defects. At our disposal, there were LuAG:Ce^{3+} single crystals with the impurity concentration of about 700 or 1400 ppm. To keep in trivalent cerium, these crystals were grown in Ar atmosphere containing hydrogen.

Gd₂SiO₅ (GSO)

Gd_2SiO_5 is crystallized in the monoclinic system with C_{2h} (P2₁/c) space group. The determined lattice parameters are the following: a = 9.1105 Å, b = 6.9783 Å, c = 6.8544 Å, β = 107.1411, V = 416.42 Å³. The cooperative influence of symmetry axis 2₁ and glide reflection along [001], located in (100) and (010) respectively, produce perfect cleavage of (100) plane and increase the separateness of (010) plane. Field distortion of the crystal lattice causes "false, incorrect" Gd-ion coordination in GSO, which does not belong to crystallographic numbers. Gd ions are located parallel to (100) plane alternating levels with 9 (C_{3v}) and 7 (C_s) coordination. The average Gd–O distance is 2.49 Å for 9-coordination, and 2.39 Å for 7-coordination.

Si ions are in a tetrahedral coordination, but differently from SiO_2, where all oxygen atoms are connected with Si^{4+},– all oxygen atoms in the GSO structure create bonds to silicon, except for the one O (O1) ion (non−silicon−bonded atoms) that join gadolinium atoms (see Fig. 3, [32]). Impurity Ce^{3+} ion preferably locates in polyhedrons with 9 coordination. Upon increasing the impurity concentratio, there appears a 30 ns component in Ce^{3+} emission, characteristic for 7-coordinated sites.
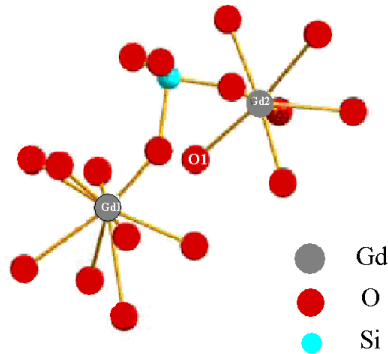
Figure 3. Gd₂SiO₅ structure [32].

GSO crystals with a diameter of up to 50 mm and a length of 150 mm were grown by the Czochralski technique in Ir crucibles at the Institute of Scintillation Materials, Kharkov, Ukraine (see [33−35] for details). Rare earth oxides Gd_2O_3, CeO_2 and SiO_2 with purity not lower than 4N mixed at stochiometric ratios were used as starting materials. The post-growth annealing of the ingots was carried out in an inert atmosphere at 1500ºC. These crystals may contain also some amount of Ce^{3+} impurity.

Polished plates of Al_2O_3, GSO and LuAG have been used for the investigations.

3. EXPERIMENTAL RESULTS AND DISCUSSION

3.1. Electronic excitations of metal oxides

Very briefly, we will consider the calculated structures of the conduction c-band and valence v-bands in α-Al_2O_3 (Fig. 4a) and similar crystals LuAG, $Y_3Al_5O_{12}$ (Fig. 4b) or GSO, Lu_2SiO_5 (Fig. 4c) [36–38]. Due to separately performed calculations for c- and v-bands, the calculated values of the energy gap (E_g) are obviously underestimated. In all the considered crystals, the top of the v-band has a small dispersion and a weakly pronounced maximum at the Γ point of the Brillouin zone, while the bottom of the c-band has more pronounced minima.

In α-Al_2O_3, the calculated value of E_g equals 6.29 and 6.31 eV for direct and indirect interband transitions, respectively [36]. However, the experimentally determined value of E_g is significantly higher, i.e. slightly above 9.4 eV at 6 K (see [39] and references therein). In α-Al_2O_3, photons of ~9.1 eV directly form excitons, which undergo unusual self-trapping at low temperatures. The fast (ns-scale) emission of self-shrunk excitons is peaked at 7.6 eV, its duration depends on the type of excitation. According to the calculations [40] and experimental results [41], the value of E_g is lower in θ-Al_2O_3 and fine-grained γ-Al_2O_3 widely used in catalyzes.
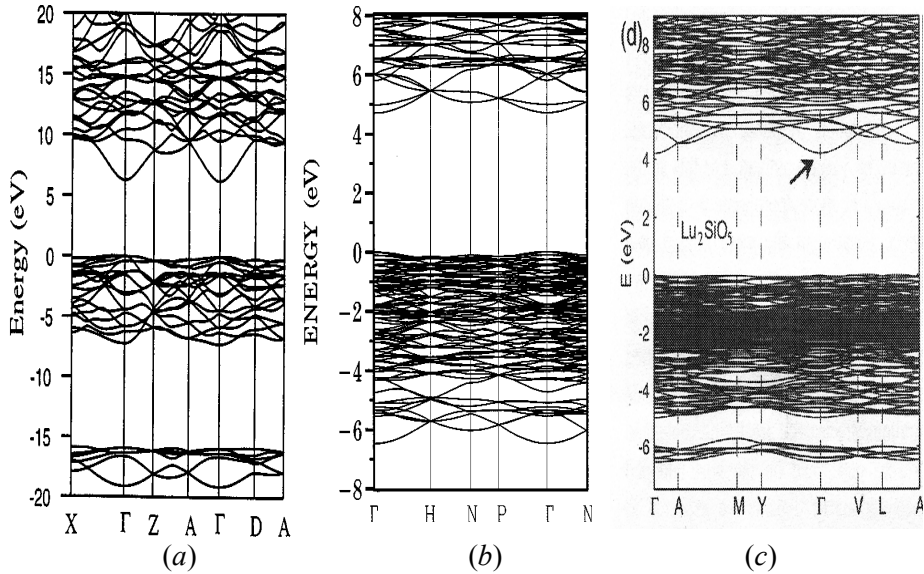
Figure 4. Electronic band structure of α-Al_2O_3 (a) [36], $Y_3Al_5O_{12}$ (b) [37] and Lu_2SiO_5 (c) [38].

By now single crystals of $Y_3Al_5O_{12}$ with 160 atoms per unit cell (isostructural with $Lu_3Al_5O_{12}$) have been thoroughly studied [19, 27, 37, 42, 43]. The width of

the v-band is slightly smaller and the value of E_g lower than those in α-Al_2O_3. It is shown also that *d*-states play essential role in the formation of the c-band. Using the methods of one- and two-photon spectroscopy, it was demonstrated that in $Y_3Al_5O_{12}$ there are several peculiarities of excitonic states, which partly overlap (in the energetic scale) with the formation region of separated *e* and *h*. At a heating of $Y_3Al_5O_{12}$, valence holes as well as conduction *d*-electrons can participate in slow hopping-type diffusion along the crystal lattice.

Fig. 4*c* demonstrates the calculated structure of c- and v-bands in Lu_2SiO_5 [38]. There is a wide v-band (4 eV) formed by 2*p*(O) states, which overlap with 4*f* states of lutetium, while the c-band contains *s*- and *p*-subbands as well as 5*d*(Lu) states with small dispersion that testifies low mobility of *d*-electrons. The interband radiative electron transition c $\rightarrow$ v at the Γ point (see arrow in Figure) superlinearly depends on the excitation intensity.

Even a general analysis of the band structure of metal oxides, serving as the object of the present thesis demonstrate their significant difference from the electronic structure of narrow-gap semiconductors with highly mobile (coherent behavior of migration) conduction electrons and valence holes or the case of wide-gap alkali halides, where valence *h* undergo self-trapping (totally lose their mobility at low temperatures), while conduction *e* preserve high (coherent) mobility even at 2 K [6, 7].

Consider next the EE in LuAG single crystals, which are widely used for many applications. Before the present study, LuAG have been already thoroughly studied, both theoretically and experimentally (see, e.g., reviews [27, 30, 44–46]). However, a further experimental study was needed for the interpretation of *e*–*h* and excitonic processes in these crystals (see also [I, II]). At our disposal, there were nominally pure LuAG single crystals grown at CRYTUR, Ltd., Turnov in reducing atmosphere and containing about 30 ppm of Ce^{3+} mainly substituting for Lu^{3+}. We used polished $4 \times 4 \times 0.8$ mm^3 plates cut off perpendicular to a growth direction.

LuAG contains a rare-earth Lu^{3+} cation with a fulfilled $4f^{14}$ inner shell and complex electron energy structure. By now the latter has been precisely interpreted only for LuF_3, $LiLuF_4$ and $LiYF_4$:Lu^{3+} [50]. In LuAG, Lu^{3+} exhibit a wide variety of discrete $4f^{14} \leftrightarrow 4f^{14}$ transitions, while interconfiguration $f^{14} \leftrightarrow f^{13}d^1$ electron transitions are expected slightly below 11 eV (such transitions are also detected at about 11 eV in garnets, see [46]).

The broadband emission with the maximum at ~5.15 eV and bandwidth about ~0.5 eV dominates in the spectra of steady-state cathodoluminescence of LuAG measured at the excitation by 5–10 keV electrons at 5–200 K. Similar to the 4.9 eV emission in $Y_3Al_5O_{12}$, investigated in details by the methods of one- and two-photon spectroscopy (see, e.g., [42, 43]), several authors (incl. us) consider the 5.15 eV emission in LuAG as the luminescence of self-trapped excitons. The considered luminescence band also dominates in the emission spectra measured at the excitation of LuAG by single ns-pulses of 300 keV electrons at 80 K. The penetration depth of such exciting electrons is ~170 μm.

So, the 5.15 eV emission has a bulk origin and is not connected with near-surface processes, which are more pronounced in the spectra of steady-state CL. The intensity of the 5.15 eV CL sharply decreases only under usage of 1−1.5 keV electrons which mainly cause the excitation of near-surface crystal regions. It is worth noting that 1 s after the 5−10-keV electron irradiation at 6 K was stopped, the intensity of the 5.15 eV intrinsic emission sharply decreased and more long-wavelength emission band peaked at ~4.5 eV is detected in the phosphorescence spectrum. The intensity of the ~5.2 eV emission decreased by at least 4 orders of magnitude (down to the noise level), while the more intense 4.5 eV emission weakened in a second by 3 orders of magnitude and continued its damping by a factor of 10 in a few minutes.

The ~4.5 eV emission detected in LuAG by many authors has a duration typical of triplet states and is ascribed by many others as the emission connected with antisite defects (AD) − Lu^{3+} ion substitutes for an Al^{3+} in octahedral coordination of oxygens, $Lu|_{Al}$. This interpretation becomes generally recognized after low-temperature growing of LuAG single crystalline films where the emission of ~4.5 eV is strongly attenuated, i.e. the amount of antisite defects is strongly decreased (see, e.g., [28, 30, 31, 44])

Fig. 5a presents the temperature dependences of the intensity of 4.50 ± 0.15 eV (antisite-related emission) and 5.2 ± 0.25 eV emissions selected though a double monochromator at the steady excitation of a LuAG crystal by 5-keV electrons (300 nA mm^{-2}). The dependence was measured at the crystal cooling with a constant rate of $\beta = 10$ K min^{-1} under the level of vacuum of about 10^{-7} Torr. The intensity of the 4.5 eV emission slightly varies at 275−135 K ($\leq 20\%$) and decreases by a factor of 2 from 130 to 6 K. On the other hand, a step-by-step increase in the 5.2 eV emission intensity occurs at the crystal cooling $300 \rightarrow 40$ K (plateaus at 220−180 and 90−70 K). The peculiarities of the ~5.2 eV emission behavior below 40 K are partly caused by the changes in the cooling rate under steady electron beam irradiation.

Fig. 5a also presents the TSL curves measured for a LuAG crystal previously irradiated by 5-keV electrons at 6 K. The curves are registered for an integral signal (1.8−6.0 eV) or for the 5.0 ± 0.3 eV emission selected through a monochromator (the latter signal is multiplied by a factor of 30). The ~200 K peak of integral TSL mainly consists of the recombination luminescence of Ce^{3+} impurity ions, a small amount of which (~30 ppm) is present in nominally pure LuAG. The emission of 5 eV is practically absent in TSL above the main peak at 87 K and a weak one at 115 K.

The thermal stability of the EPR signal of the assumed self-trapped holes (in a form of O^- ions) was investigated in a LuAG single crystal doped with Sc^{3+} ions [27]. Pulse annealing of the EPR signal occurs between 75 and 140 K. However, according to [45], this EPR signal was not found in nominally pure LuAG crystals without scandium impurity ions (including the objects of the present study).
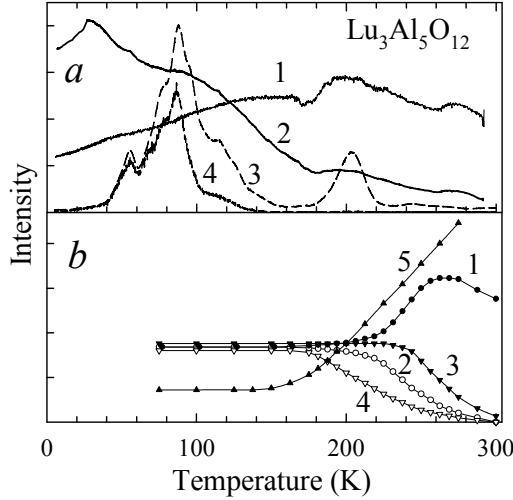
Figure 5. (*a*) Temperature dependences of the intensity of 4.5 (1) and 5.2 eV emission (2) at the excitation of LuAG by 5-keV electrons (300 nA mm^{-2}). TSL curves measured ($\beta = 10$ K min^{-1}) for an integral signal (1.8−6.0 eV, curve 3) or for the 5.0 eV emission (4, multiplied by a factor of 30) in a LuAG crystal previously irradiated by 5-keV electrons at 6 K.

(*b*) Temperature dependence of short (1, 2) and long (3, 4) components of the 5 eV emission as well as of Ce^{3+} emission (2.4 eV, curve 5) at the excitation of LuAG by single nanosecond electron pulses (3 ns, 300 keV, 80 A cm^{-2}). The emission pulse amplitude (1, 3, 5) or emission integral (2, 4) were registered. See the text for details.

We have studied the kinetics of luminescence bands in the region of 1.9−6.0 eV at the excitation of LuAG crystals by single electron pulses at 80−300 K (3 ns, 300 keV, 80 A cm^{-2}, a 30 s pause between two sequential pulses). Of particular interest were the broadband emissions peaked at 4.5 eV (related to Lu|$_{Al}$ antisite defects) and ~5 eV in LuAG crystals. Similar to the 4.9 eV emission in YAG [42, 43], the ~5 eV luminescence in LuAG is tentatively ascribed to unusual excitons with the radius smaller than the size of a unit cell containing 160 atoms. Any emission kinetics can be described by two exponents with different τ (further on these components will be reported as "short" and "long"). The decay times for ~5 eV emission at 80 K equal 0.5 and 1.6 μs, while a crystal heating to RT causes the shortening of a short component down to 9 ns.

Fig. 5*b* presents the temperature dependence of the 5 eV emission at the excitation of LuAG by single nanosecond electron pulses (see also [II]). In contrast to the inertial recombination TSL of 5 eV that is practically vanished above 130 K, the integral ($A \times \tau[T]/\tau[80$ K]) of a long component of the 5 eV emission remains constant till ~160 K and starts to decrease above this temperature. The integral of a short component decreases at $T > 225$ K. The decrease of a pulse amplitude A for the long 5 eV emission occurs above 240 K, while the

22

value of A for a short component increases at 220–260 K and only then decreases at $T > 275$ K. According to Fig. 5b, the efficiency of 2.4 eV Ce^{3+} emission (about 30 ppm of Ce^{3+} ions in our LuAG sample) is low at the electron-pulse excitation at 80–140 K ($\tau \sim 50$–60 ns) and A starts to increase in the temperature region where the 5.0 eV TSL is quenched, in parallel with the rise of τ up to 100–130 ns.

The analysis of the experimental presented data agrees with the attribution (see [27] and more solid evidence related to ~4.9 eV emission in YAG [42, 43]) of the ~5.1 eV emission in LuAG to unusual excitons of small radius. The specific character of the motion of such excitons is determined by the possible hopping diffusion of small-radius hole polarons inside a complex oxygen sublattice. In metal oxides, peculiarities of the behavior of hole polarons have been discussed over a long time (see, e.g., [43, 47–49]). The values of activation energy and frequency factor have been determined for TSL peaks at 80–150 K in LuAG:Ce^{3+} [45]. However, in our opinion, the obtained enormously low values of $p_0 = 10^9$–10^{11} s^{-1} can not be explained only by a large number of hops of a hole polaron needed to reach a luminescence center, and probably are connected also with the frequency of a hoping diffusion of "heavy" small-radius polarons or with tunnel recombination of e–h oriented along definite directions.

The creation spectra of some TSL peaks by VUV radiation have been measured for the purpose of separating the contribution of oxygen and lutetium (cation) excitons or separated e and h to the transformation/creation of defects in LuAG crystals. The crystal was irradiated by an equal quantum dose of VUV radiation (~10^{13} photons cm^{-2}) from a hydrogen discharge source at each of several energies (7.5–11.5 eV) at 80 K. The reference signal for normalization was recorded from sodium salicylate. TSL was measured with $\beta = 10$ K min^{-1} and the light sum (or peak intensity) of a TSL peak was taken as a measure of the centers created by VUV radiation and responsible for this peak. Fig. 6 shows the creation spectra of the TSL peaks at 90 and 115 K connected with hole centers in LuAG. The figure also presents the reflection spectrum measured for the same sample using SR of 7–13 eV at 80 K. The creation efficiency of the TSL peaks starts to rise at 7.5 eV testifying to the beginning of a weak ionisation. Similar to YAG [42], the rise of the ionisation efficiency at 7.6–8.0 eV reproduces the Urbach tail of exciton absorption in LuAG at 80 K.

The spectra of two-photon absorption (TPA) can provide important information on intrinsic EE in strictly oriented LuAG single crystals. Unfortunately, at present there exist only the TPA spectra measured in our laboratory in Tartu at 80 or 300 K for high-quality YAG crystals grown by the method of oriented crystallization in Russia. It was mentioned already that YAG and LuAG are isostructural materials. A comparison of the spectra of one and two-photon absorption was performed for YAG [42, 43]. At 80 K, two narrow peaks at 7.2 and 9.0 eV have been detected in the spectrum of TPA. The second peak is situated in the region of exciton absorption band in α–Al_2O_3, where aluminium ions occupy octahedral interstitial sites in the closely packed oxygen lattice. At

the same time, the first peak of TPA is found at a significantly higher energy than the exciton absorption band in Y_2O_3. In a unit cell of YAG, 16 Al^{3+} ions are located at octahedral sites (C_{3i} symmetry) while the other 24 aluminium ions are within oxygen tetrahedrons. Specifically, tetrahedral aluminium-oxygen clusters are responsible for a long-wavelength region of the TPA spectrum in YAG. Isostructural LuAG crystals exhibit very close spectral characteristics.
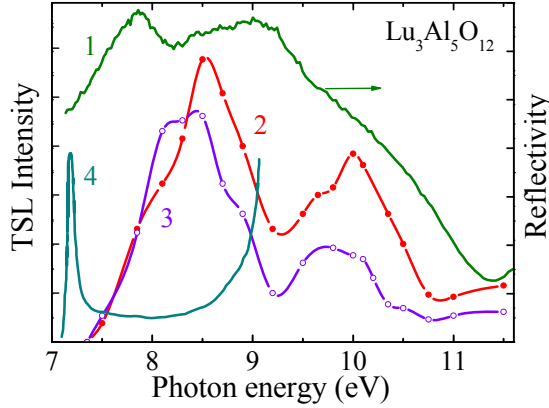

Figure 6. Reflection spectrum (curve 1) measured for a LuAG crystal using SR at 80 K. The creation spectra of the TSL peaks at 115 K (2) and 90 K (3) measured for LuAG after isodose VUV irradiation at 80 K (see the text for details). Two-photon absorption spectrum for YAG at 80 K, [42, 43] (curve 4, see text for details).

Returning to the creation spectra of TSL peaks by VUV-radiation in LuAG (see also [II]), we can note that the creation efficiency of the TSL peaks at 90 and 115 K is low in the regions related to the excitation (not ionisation) of tetrahedral aluminium complexes (7.4–7.5 eV) as well as of the octahedral ones (~9.2 eV). The third region (10.5−11.5 eV) where recombination luminescence (TSL) is weakly excited coincides with the region of efficient $f^{14} \leftrightarrow f^{13}d^1$ electron transitions in Lu^{3+} (these transitions have been recently investigated in metal fluorides (see [50] and references therein). The irradiation of LuAG with the photons that form lutetium cation exitons does not lead to the efficient excitation of recombination TSL.

3.2. Radiation effects in LuAG

A comparative investigation of reflection and absorption spectra, as well as different luminescent characteristics has been performed for LuAG single crystals − virgin or previously irradiated with 2.14 GeV ^{238}U ions (fluence of

10^{12} ions/cm^2) at RT. It was rather difficult to use a direct method of optical absorption at higher fluences.

Fig. 7 presents the reflection spectra measured for virgin and ^{238}U-irradiated LuAG single crystals using SR of 5−19 eV at 10 K. In the irradiated sample, reflection increases in a wide region, below the energy gap and especially above it, when a nearly normal reflection from a virgin sample is low. Increased reflection is caused by radiation-induced complex structural defects, which are differently oriented with respect to incident SR.
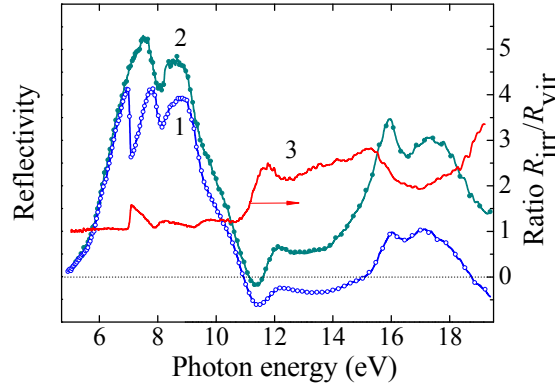
Figure 7. Reflection spectra (normalized at a long-wavelength tail) measured for a virgin LuAG single crystal (curve 1) and the sample previously irradiated with ^{238}U ions (2.14 GeV, 10^{12} ions cm^{-2}, RT, curve 2) using synchrotron radiation at 10 K. The ratio of the reflection spectra for irradiated and virgin samples (curve 3).

Fig. 8 shows the optical absorption spectra measured at RT for virgin and uranium-ion-irradiated LuAG crystals (with ~30 ppm of Ce^{3+}) at RT. The range of ^{238}U ions was about 50 μm (see Section 2.1). The radiation-induced optical absorption (RIOA, difference between the spectra after and before irradiation) is especially high at 6.0−6.6 eV and at $hv > 7.2$ eV. This difference spectrum consists of well-known bands related to F and F$^+$ centers (peaked at 6.05 and 5.4, 3.5 eV, respectively [27, 29, 45, 51]). So, the sample kept after ion-irradiation for a month in darkness and without any exposure to an atmosphere still contains a certain amount of radiation-created F and F$^+$ centers. The last conclusion is clearly supported by the excitation spectra measured at 10 K for the 2.8 eV emission of F centers and 3.15 eV emission of F$^+$ centers in the LuAG previously irradiated with ^{238}U ions (see Fig. 8). The figure also presents the excitation spectrum for a broadband emission peaked at ~4.5 eV, which is conclusively interpreted in the literature as the emission related to antisite defects $Lu|_{Al} - Lu^{3+}$ ion at Al^{3+} site [27, 45].
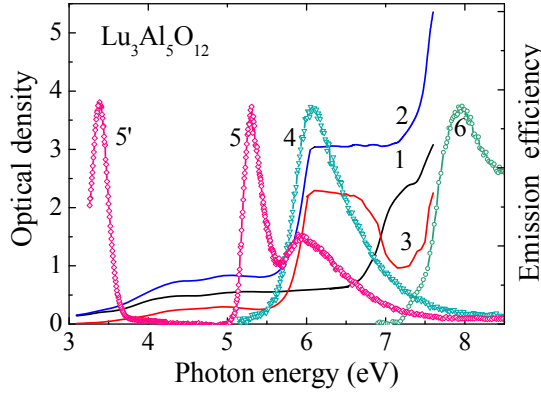
Figure 8. Optical absorption spectra measured at RT for virgin (curve 1) and uranium-ion-irradiated (2.14 GeV, 10^{12} ions cm^{-2}, RT, curve 2) LuAG crystals (~30 ppm of Ce^{3+}) at RT. The difference between the absorption spectra after and before irradiation (3). The excitation spectra measured at 10 K for the 2.8 eV emission of F centers (4), 3.15 eV emission of F^+ centers (curves 5 and 5') and 4.5 eV emission (curve 6) of Lu$|_{Al}$ antisite defects related emission in LuAG previously irradiated with ^{238}U ions.

The analysis of the data presented in Figs. 7 and 8 allows us to conclude that the additional numbers of F, F^+ and Lu$|_{Al}$ centers are created by the irradiation of LuAG with SHI, more than 99% energy of which is transferred to an electron subsystem of a crystal. According to theoretical calculations [52], the formation energy for an AD in LuAG is lower than that for a Frenkel pair. So, the efficient creation of AD is expected under irradiation of LuAG with SHI providing an extremely high density of EE within ion tracks (LET > 20 keV/nm). Besides a relatively small amount of as-grown single AD (excitation band for such AD-related emission of ~4.5 eV lies at 6.9–7.3 eV, see Fig. 9), a superhigh-dense SHI-irradiation can cause also the creation of a pair or even triple AD. The optical characteristics of such complex AD should be significantly different from those for single antisite defects. The excitation spectrum for 4.5 eV emission in a SHI-irradiated LuAG (ion range ~50 μm) at 10 K contains a well-pronounced band peaked 7.9−8.0 eV. In is worth noting that the AD-related emission efficiency (as well as other emissions) is significantly attenuated in the irradiated sample, partly due to reabsorption effects. Two-AD containing center (Lu$|_{Al}$−Lu$|_{Al}$) has a complex structure with strong anharmonicity. As a result, there should be an increased probability of nonradiative transitions from the excited state of a complex AD center even at low temperatures. It is notable that "impurity AD" − a Ce^{3+} impurity ion (its radius is by 14% larger than that of Lu^{3+}) located at an Al^{3+} site in an octahedral coordination are also detected in LuAG single crystals (see also Section 3.4).

The manifestations of radiation-induced defects can be also seen in the reflection spectra of LuAG crystals. The ratio of the reflection spectra for the

SHI-irradiated and virgin LuAG samples R_{irr}/R_{vir} is shown in the Fig. 7 (curve 3). The value of R_{irr}/R_{vir} at $h\nu = 15-16$ eV is about three times as high as at $6-6.9$ eV, where this value is close to unity. It is necessary to stress that one of the main reflection maxima in α-Al_2O_3, where all Al^{3+} ions are located in an octachedral coordination, is located at 16 eV (see [36], 10 K). An especially sharp rise of R_{irr}/R_{vir} occurs at $11.5-12$ eV that is close to the region where $f^{14} \leftrightarrow f^{13}d^1$ interconfiguration electron transitions in Lu^{3+} are expected. Ion-induced defects can change a local symmetry near regular Lu^{3+} sites, thus increasing the transition probality of Lu^{3+} into an excited state. A pronounced ratio peak at 7.1 eV and a peculiarity at $7.9-8.0$ eV can be connected with the formation region of single and pair antisite defects (see Fig. 9). The excitation band for AD-related emission ($\sim 4.5-4.7$ eV) nicely coincides with this peak of R_{irr}/R_{vir} (Fig. 9). Unfortunately, some ambiguity of the interpretation of radiation-induced changes in reflection spectrum still remains due to possible contamination of the crystal surface at the ion irradiation.
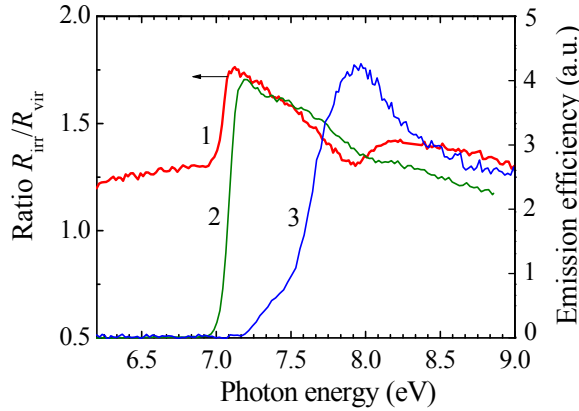

Figure 9. Ratio $R_{irr}/_{vir}$ (1) for ion-irradiated and virgin sample (see also Fig. 7) and the excitation spectra for 4.7 eV emission in a virgin (2) and for 4.5 eV emission in SHI-irradiated LuAG sample (3) measured at 10 K. Curve 3 is multiplied by a factor of 20.

Fig. 10 demonstrates the emission spectra (pulse amplitude A was registered) measured at the excitation of virgin and ion-irradiated LuAG crystals (30 ppm of Ce^{3+}) by single electron pulses (300 keV, 3 ns, 80 K). Besides Ce^{3+} luminescence (2.4 eV), the emissions related to self-trapped excitons (~ 5.1 eV) and AD (~ 4.5 eV) are distinguished in the spectrum for a virgin LuAG. The irradiation of LuAG with SHI weakens the emission at $4.3-5.3$ eV by a factor of 5. The emission was collected from the irradiated crystal surface and its weakening is partly caused by a substantial reabsorption in the 50-μm ion-irradiated layer, while the range of incident 250-keV electrons (average energy) was about

150 μm. The enhancement of the emission peak amplitude is detected only at 3.25–4.25 eV. There are two maxima of this enhanced emission (curve 3) – the main component at ~3.75 eV and a weak one at ~4.05 eV. The absolute enhancement of the emission at ~3.75 eV was detected due to its short decay time (~70 ns) at 80 K. The emission undergoes reversible (typical for intracenter luminescence) thermal quenching already at 125 K (see insert in Fig. 10). If the opposite, nonirradiated surface of LuAG (thickness ~1 mm) is excited by electron pulses, there is no ~3.75 eV emission at all. The possible origin of this emission will be considered in Section 3.4.
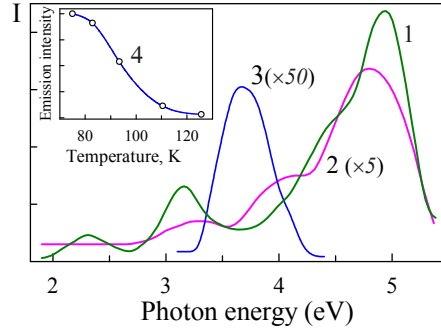
Figure 10. Emission spectra (pulse amplitude *A* was registered) measured at 80 K for a virgin (1) or a SHI-irradiated LuAG crystal (2.14 GeV, 10^{12} ions cm^{-2}, RT, curve 2). The enhancement of emission peak amplitude in an ion-irradiated crystal (3). Inset shows the temperature dependence of the 3.7 eV emission (curve 4) excited by single electron pulses (3 ns, 300 keV).

We have studied the thermal annealing of optical absorption for a LuAG crystal irradiated with swift uranium ions with energy of 2.14 GeV at RT (see also [I]). The spectra of optical absorption were measured at RT before and after irradiation with SHI. The difference between these two spectra is considered radiation-induced optical absorption (RIOA), the annealing of which in different temperature regions is presented in Fig. 11. A step-by-step regime of thermal annealing was performed in a very dry air atmosphere (see Section 2.1), all the absorption spectra in the region from 1.5 to 8 eV were measured at RT.

The annealing of F-type-center absorption band (6.1 eV) seems to be gradual, starting from room temperature (we do not have exact information, because absorption coefficients were above the measurement limit). The final stage of the annealing occurs at 800−1000 K, $(0.34–0.40)T_{\text{melt}}$. Absorption at 6.7 eV (this band revealed itself during annealing procedure) decreases at slightly higher temperatures, i.e. at 1100−1150 K. The 7.2 eV-band related to AD undergoes annealing at approximately $0.5\,T_{melt}$, where the intensive ionic movement takes place already. And only beyond $0.6\,T_{melt}$ we can see the annealing of 5.3 (5.0), 4.4 eV and 3.5 eV bands. It is hard to say exactly, which de-

fects these bands are connected with, because there is a clear strong overlapping of different absorption bands. As the annealing of the bands at 3.5−5.5 eV takes place at such high temperatures, we can suppose their (at least partially) connection to some complex, aggregate centers, which are formed during SHI-irradiation.
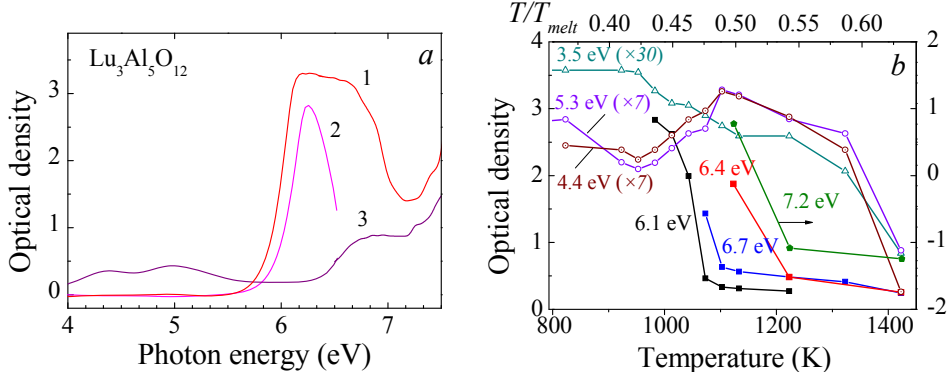

Figure 11. *(a)* The spectrum of RIOA for $Lu_3Al_5O_{12}$ irradiated by U^{238}-ions (2.14 GeV, 10^{12} U/cm^2, RT, curve 1). The decrease of RIOA caused by the preheating of the crystal from 1043 to 1073 K (curve 2), and 1123$\rightarrow$1423 K (3). *(b)* The dependence of the RIOA measured for a given region (marked in the figure) on the preheating temperature. Some curves are multiplied by an indicated factor.

The irradiation of α-Al_2O_3 at RT with ^{238}U ions (2.4 GeV, 10^{12} ions/cm^2, ion range $R = 90$ μm) causes the creation of F centers (absorption at 6.0 eV, emission at 3 eV), F^+ centers (absorption at 4.8, and 5.4 eV; emission at 3.8 eV) [53, 54] and more complex defects (see also [III, V]).

Fig. 12*a* shows the RIOA spectra measured after ion-irradiation at RT or after an additional preheating to a certain temperature T_{pr}. The absorption band of F centers dominates in the RIOA spectrum, while the absorption related to F^+ centers is significantly lower. Fig. 12*b* presents the annealing curves OD(T_{pr}) constructed on the basis of these spectra for the absorption at 6.5 eV as well as of F (6.0 eV) and F^+ centers (4.8 eV). In Al_2O_3 ($T_{melt} = 2345$ K), more than a half of radiation-created F centers is annealed at 500−750 K, about a quarter − at 800−900 K, while only the heating to 1400 K provides the total destruction of the RIOA. The annealing of F centers in pure α-Al_2O_3 crystals irradiated by 14-MeV neutrons ends by 900 K [55]. The defects stable even at 0.64 T_{melt} and responsible for the RIOA at $\geq$6.4 eV are tentatively formed in the crystal regions nearby the core of ion tracks. According to [23], it is rather difficult to anneal the complex centers of light scattering − radiation-induced negative crystals − in ruby crystals, α-Al_2O_3:Cr^{3+}.
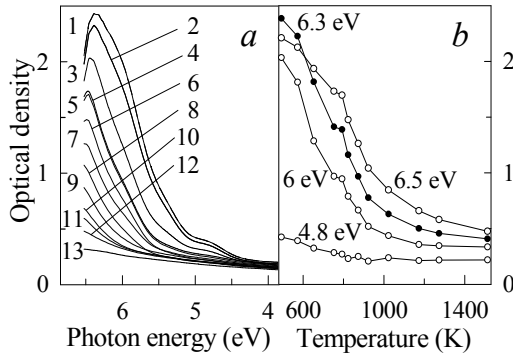
Figure 12. *(a)* The spectra of optical absorption at 295 K for Al_2O_3 irradiated by 2.4-GeV ^{238}U ions (10^{12} ions/cm^2) at RT and preheated to 483 K (1), 573 K (2), 653 K (3), 753 K (4), 793 K (5), 823 K (6), 873 K (7), 923 K (8), 1023 K (9), 1173 K (10), 1273 K (11), and 1513 K (12), (13)-before irradiation. *(b)* The annealing of optical absorption at 4.8, 6.0, 6.3, 6.5 eV.

In α-Al_2O_3 crystals irradiated by fast neutrons the impact (knock-out) mechanism was considered as the main reason for radiation damage [56]. X-rays do not cause the coloration of stoichiometric α-Al_2O_3, while the efficient defect creation takes place in the heavy-ion-irradiated samples due to non-impact processes, e.g., via hot recombination of electrons and holes under the conditions of high density of EE in the ion tracks.

Fig. 13 shows the spectrum of the RIOA, which can be annealed by the heating of an ion-irradiated sample from 493 to 573 K. The absorption bands annealed in this temperature range are mainly connected with F and F$^+$ centers. The majority of F and F$^+$ centers can be annealed by heating to 823 K, while the subsequent heating 823$\rightarrow$873 K (i.e. up to about 40% of the melting point) causes the decrease of absorption bands at 5.8−6.55 eV. The origin of the centers responsible for the high-energy absorption bands is still unclear.
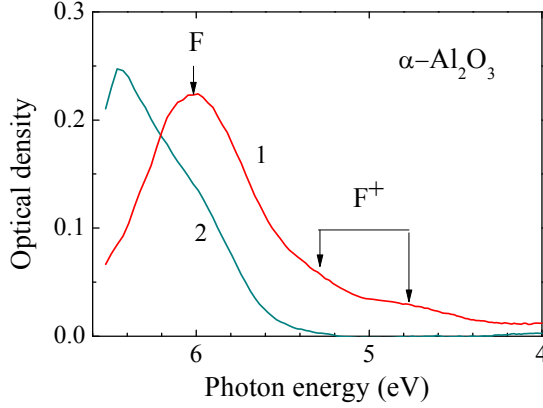
30

Figure 13. Induced optical absorption annealed due to the intermediate preheating 493→573 K (curve 1) and 823→873 K (2) in an α-Al$_2$O$_3$ crystal previously irradiated with 2.2 GeV U^{238} ions (fluence of 10^{12} ions/cm^2) at RT. All the spectra after preheating to a certain temperature were measured at 295 K.
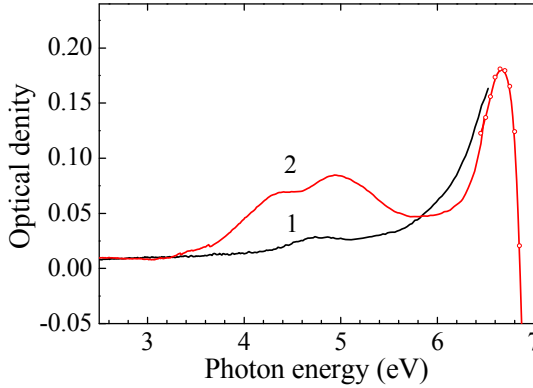

Figure 14. RIOA of Al$_2$O$_3$ (curve 1) and LuAG (2) remained after preheating of the SHI-irradiated samples to 1423 K (LuAG) or 1513 K (Al$_2$O$_3$).

Comparing the RIOA annealing in α-Al$_2$O$_3$ and LuAG, we can conclude that the annealing processes for some defect types are similar (e.g. F centers), for some others − different. In both crystals, a part of RIOA remains stable even after preheating to a rather high temperature (see Fig. 14). It is worth noting that the 6.7 eV band is clearly detectable after preheating to 1423 K($\sim$0.64 T_{melt}).

Searching for low-temperature line emission of large-radius excitons in LuAG and ruby crystals, virgin and ion-irradiated, we detected instead through a double vacuum monochromator at 6 K a typical emission of H$_2$ molecules captured in cavities (negative crystals). Hydrogen molecules serve as centers of efficient light scattering.

31

3.3. Radiation damage related to the collapse
of discrete breathers

In metals and alloys, radiation damage is mainly caused by the knock-out (impact) mechanism connected with elastic collisions of high-energy incident particles (neutrons, protons, ions) with the atoms of a crystal. In a number of WGM, besides a rapid impact mechanism, the second, slower adiabatic mechanism of FD creation connected with the excitation and ionisation of an electron subsystem plays an essential role as well. The need to analyse the processes causing radiation damage in metals, semiconductors and dielectrics (WGM) under their irradiation providing an extremely high density of EE (e.g., in the tracks of GeV-SHI) led theorists to the suggestion of a novel, the third mechanism of structural defects creation as well as destruction of solids in the framework of a nonlinear interaction of electronic excitations with lattice vibrations in the materials predisposed to anharmonicity.

According to theoretical predictions, a new kind of intrinsic localized mode with a large amplitude and frequency above the top of the acoustic phonon spectrum may exist under the dense excitation of a crystal lattice predisposed to anharmonic interactions [17−20]. These unusual excitations, also referred to as discrete breathers or discrete solitons, are expected to be especially strong in the WGM built up of ions with very different masses − the frequency of discrete breathers can fall in a gap between acoustic and optical vibration branches.

In wide-gap complex metal oxides with $E_{FD} > E_g$ and many atoms per unit cell (e.g., $Y_3Al_5O_{12}$, $Lu_3Al_5O_{12}$, Y_2SiO_5, Gd_2SiO_5), the contribution of all the three defect creation mechanisms (knock-out, decay of EE, breathers-related) can be expected at the irradiation with SHI providing an overlapping of cylindrical ion tracks (at a fluence of 10^{12} ions/cm^2, the average distance between tracks is about 10 nm). On the other hand, the third mechanism of radiation damage is supposed to be inefficient in the binary pure MgO crystals with $E_{FD} > E_g$ and close masses of anions and cations.

The necessity to take into account the nonimpact creation mechanisms (besides the knock-out one) of FD, their elementary associations as well as of a more complex radiation damage has been demonstrated even for binary wide-gap crystals irradiated by ~GeV SHI with a fluence of 10^{11}–10^{13} ions/cm^2 using more sensitive methods of thermoactivation and low-temperature VUV-spectroscopy (see, e.g., [V, 57]). Radiation defects and electronic excitations of crystalline and glassy SiO_2 have been investigated in detail [58, 59].

Some tentative manifestations of the third, breather-related mechanism of radiation damage were detected by us in LuAG crystals (mass ratio Lu/Al= 175/27 = 6.5) irradiated with SHI. However, a significant enhancement of the creation of temperature-stable 3D radiation damage via the third, theoretically predicted mechanism [17−20] is expected in complex Gd- and Y-oxyortho-silicates. In the Gd_2SiO_5 (GSO) with high values of mass ratio Gd/O = 10 and Gd/Si = 5, there are favorable conditions for the predicted effects in anharmonic systems. The characteristics of the EE in a VUV spectral region and the lumi-

nescence processes in nominally pure and Ce-doped GSO were studied in [60−63].

Figure 15a presents the data on the annealing of the RIOA in the GSO irradiated with 2.04-GeV gold ions (10^{12} Au/cm^2, RT). Similar to LuAG, a pulsed regime of thermal annealing was used. A significant part of RIOA at 5.75 eV is annealed between two subsequent preheating cycles to 973 and 1123 K. Comparing with SiO_2, we can suppose, that 5.75 eV in GSO band could be analogous to the so called E'_γ-center (absorbing at 5.83 eV, dangling Si bond, which could be a part of the oxygen vacancy) of silica with $E_g \sim 9$ eV, [58, 59] (in GSO $E_g > 6.8$ eV) [60−63]).
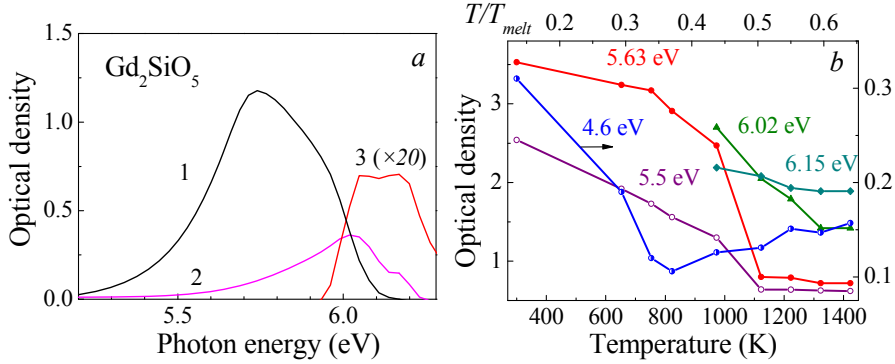

Figure 15. *(a)* Difference spectra of RIOA caused by the preheating of the SHI-irradiated Gd_2SiO_5 crystal (2.04 GeV, 10^{12} Au/cm^2, RT) from 973→1123 K (1), 1223→1323 K (2) and 1323→1423 K (curve 3, multiplied by a factor of 20). All the spectra are measured at 295 K. *(b)* The dependence of the RIOA of GSO measured for a given region (marked in figure) on the preheating temperature.

The absorption bands 6.02 and 6.15 eV in GSO could be similar with the 6.5-6.7 eV band in SiO_2, which is a $\equiv Si - O - O - Si \equiv$ peroxy linkage,– kind of an interstitial oxygen [59]. The oscillator strength of this band in SiO_2 is small, and the intensity of similar absorption bands in GSO is also relatively low.Figure 15b shows the dependences of the selected optical absorption at 5.5– 6.15 eV on the preheating temperature. In GSO, we can measure RIOA at 6.02 and 6.15 eV only after preheating of the irradiated samples up to $0.44T_{melt}$, because the value of OD exceeded the experimental limit at lower temperatures. The absorption at 5.55 and 5.63 eV gradually decreases already at a relatively low temperature that is typical of the defects formed via $e-h$ recharging processes. The situation is similar with the annealing of the majority of defects in SiO_2. The absorption band at 4.6 eV band is similar to a non-bridging oxygen hole center (NBOHC) in SiO_2 absorbing at 4.8 eV. Both bands disappear at 700 K (for GSO see Fig. 16). In SiO_2, the decomposition of 4.8-eV-related defects oc-

curs due to the recombination with H or H_2 molecules, which are mobile at 80 and 200 K, respectively [59]. If 6.02, 6.15 eV bands in GSO are really connected with oxygen interstitials (similarity with 6.4−6.7-eV absorption in SiO_2) then they also disappear almost in the same T_{melt} region − $0.58\,T_{melt}$ is needed for GSO, as for SiO_2 − $0.5\,T_{melt}$ (6.4−6.7 eV band). Using 5.68 or 5.9 eV photons to excite irradiated or virgin GSO crystals, we have approximately the same emission spectra (a new emission is not observed after irradiation with [197]Au ions). In SiO_2, E_γ' defects (dangling Si bond, ≡Si•, absorption at 5.8 eV) are not luminescent centers either.

Preheating to 1423 K causes relatively small changes in the optical absorption at 6.2−6.5 eV, which is measurable using a double monochromator. Unfortunately, at this point we did not succeed in measuring the absorption spectra at $h\nu > 6.5$ eV with a necessary accuracy via an ordinary VUV monochromator with a high level of scattered light. However, a part of the RIOA related to 3D nanosize defects also remains in this spectral region after preheating to 1423 K (limit of our measurements). It is worth noting that the emission of hydrogen molecules (~10 eV) was detected in the cathodoluminescence spectrum measured at 6 K for an SHI-irradiated GSO crystal (~2 GeV, 10^{12} ions/cm^2). These molecules fill in nanocavities created during SHI-irradiation and cause light scattering that hinders the measurements of radiation-induced optical absorption.
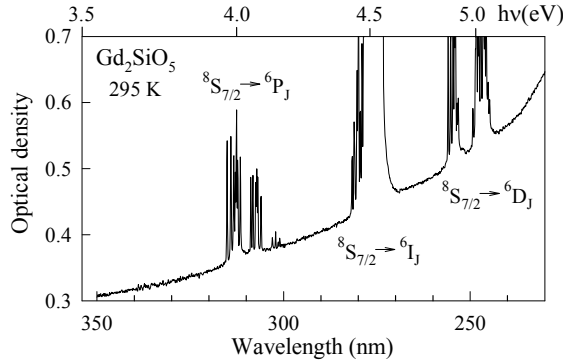

Figure 16. Absorption spectrum measured at 295 K for a Gd_2SiO_5 crystal irradiated with [197]Au-ions (2.04 GeV, 10^{12} Au/cm^2, RT) and additionally annealed to 1423 K. Resolution of a double monochromator is 0.1 nm

Similar to LuAG, the annealing of SHI-irradiated GSO to $0.6\,T_{melt}$ destroys all the defects formed during irradiation via the $e−h$ recharging of impurity and as-grown defects, while some complex radiation damage still remains. The latter causes an increase of the background due to the enhanced light scattering even far away from the fundamental absorption. However, the situation is rather different in a high-energy region of $^8S_{7/2} \rightarrow {}^6I_J$ and $^8S_{7/2} \rightarrow {}^6D_J$ transitions in Gd^{3+} − there is a sharp rise of scattered light even for the absorption measurements with a double monochromator, which significantly suppresses scattered light with all

frequencies except for the incident photon (see Fig. 16). A large-size radiation damage stable up to pre-melting temperatures is responsible for this light scattering.

In LuAG, the annealing of many defects is efficient only at $(0.4–0.5)T_{melt}$, when ions became mobile. However, there is a much closer similarity in a GSO–SiO_2 pair, as compared to Al_2O_3–LuAG. We assume, that NBOHC have the same structure in GSO and SiO_2, E`$_\gamma$ center composition is also similar in these two crystals.

Let us discuss briefly the possible experimental manifestations of the third mechanism of radiation damage in GSO and LuAG (but we did not detect such manifestation in binary MgO) that is connected with the formation of intrinsic 3D defects − a relatively large group of host ions that underwent a rearrangement under a superhigh excitation density in the cylindrical tracks of SHI (~2 GeV, [238]U or [197]Au, 10^{12} ions/cm^2). Along an ion track, about 99% of the SHI energy is spent on the excitation of an electron subsystem, and only close to the end a slowed down bombarding particle creates FDs and their nanosize associations due to the knock-out mechanism. This damaged part of a lattice at the end of the ion path tentatively serves as a certain wall for a mobile discrete soliton formed in the track with the frequency above the acoustic phonon branch. Back reflection from this wall is followed by interference between the breathers moving in opposite directions. As a result, we have a set of lattice points with an increased vibration amplitude and anharmonicity.

The conditions for localization and collapse of discrete solitons are theoretically considered (see [20] and references therein). One-dimensional solitons do not undergo a collapse, while the possibility of the collapse of 2D or 3D solitons depends on many parameters, in particular, on the mass ratio for the heavy and light ions in a particular material, and on the presence of the energy gap between the acoustic and optical branches in a phonon spectrum. In Gd_2SiO_5, the mass of gadolinium (157) exceeds the masses of silicon and oxygen by a factor of 5.6 and 9.8, respectively. Among alkali halides, the value of the mass ratio is high in NaI, I/Na = 5.5 and this value is enormously high (I/Li ~18) for LiI. In LiI and NaI, significant peculiarities in the interaction of EE with lattice vibrations were experimentally detected [64, 65] and interpreted by theorists as mani festations of discrete breathers. There are no similar peculiarities in KCl and MgO, where the mass ratio is close to unity (0.8 and 0.67 respectively), and the acoustic and optical vibration branches overlap [66].

Some of our experimental data obtained in complex metal oxides under irradiation with SHI (~2 GeV, fluence $\Phi = 10^{12}$ ions/cm^2, average distance between tracks ~10 nm) providing an extremely high density of EE (> 30 keV/nm) can be considered as possible manifestations of the collapse of solitons with the creation of intrinsic nano- and mesodefects. The ion-irradiation (fluence of up to 3×10^{13} ions/cm^2) of highly pure and perfect MgO single crystals does not cause the creation of nano- and mesodefects, the presence of which is supposed to cause the cracking of the crystal during its consequent annealing to high tem-

peratures, $T > 0.7\,T_{\mathrm{m}}$. Both radiation-induced optical absorption and strong light scattering were detected after the irradiation of Gd_2SiO_5 by SHI with a fluence starting from 3×10^{11} ions/cm^2, while an especially sharp rise of scattered light at $h\nu = 5.5$–6.5 eV was registered after irradiation with $\Phi = 10^{12}$ Au/cm^2 even for the absorption measurements using a double monochromator, which significantly suppresses scattered light. A careful separation of optical absorption from scattered light was performed earlier for laser media materials (ruby and saphire) [23]. We did not succeed yet in such separation in Gd_2SiO_5 irradiated with ~GeV SHI. It was mentioned in Section 3.2 that a step-by-step annealing of SHI-irradiated LuAG up to $0.63\,T_{\mathrm{m}}$ did not totally remove radiation-induced absorption and scattering. The presence of the remaining radiation-induced absorption in LuAG and GSO at $h\nu > 6.5$ eV is confirmed also by a comparative analysis of the cathodoluminescence spectra (penetration depth of 15-keV electrons is ~10 µm) measured through double monochromators with a low level of scattered light at 6 K for virgin crystals and the SHI-irradiated samples preheated to 1423 K.

According to Vaisburd [11−13], the creation of 3D nanosize defects via the third creation mechanism is accompanied by the appearance of novel emissions. A novel ultra-fast luminescence from incipient ion tracks of insulator crystals was also revealed in [67]. A theoretical consideration and some experimental manifestations of the third mechanism of radiation damage in $Y_3Al_5O_{12}$ exposed to a high uniaxial stress are presented in [19]. The experience in the investigation of metal alloys exposed to high-dense and prolonged irradiation convincingly shows that radiation-induced nano- and mesodefects (3D defects) formed due to a rearrangement of many host ions cannot be destroyed, in principle, by annealing even to pre-melting temperatures.

3.4. Influence of impurities on radiation resistance

Insufficient radiation resistance is a serious limitation for WGM ($E_{\mathrm{g}} = 5$–15 eV) possessing other necessary properties to be practically used as fast and effective scintillation detectors and selective dosimeters for medical and industrial purposes, spectral transformers for mercury-free fluorescence lamps and displays, etc. No success in future industrial fission reactors can be achieved without a significant enhancement of the radiation resistance of construction and diagnostics materials.

The energy absorbed by the material during irradiation is only partly transformed into useful luminescence, while a significant part of the energy is transformed by non-radiative transitions via heat release or the creation of radiation-induced Frenkel defects − vacancies and interstitials − including long-lived pairs, which are stable during hours and days, and play a crucial role in the material degradation. The ratio between three transformation channels depends on many factors, such as temperature, concentration and spatial distribution of lu-

minescence centers (especially important is the presence of pairs of heavy impurity ions) as well as on the density of electronic excitations.

In principle, the radiation resistance of some WGM can be increased by a light doping due to the so-called solid-state analogue of the Franck-Hertz effect revealed in alkali halide crystals doped with Tl^+ and Ag^+ impurity ions, which have both ground and an excited state energy levels within an energy gap (see [68, 69]). If the energy of a hot conduction electron, formed at the absorption of an exciting photon, is not sufficient for electron-electron scattering with the creation of a secondary electron-hole pair, the hot e can spend its energy excess for the direct excitation of an impurity center up to a triplet excited state, while a subsequent recombination of the cooled conduction electron with a valence hole does not create a Frenkel pair. So, the Franck-Hertz effect is some kind of "luminescent protection" against radiation damage, caused via hot electron-hole recombination in materials with $E_{FD} > E_g$ (see [70–72, IV]). Just such energetic inequality is valid for many complex two- and trivalent metal oxides (see, e.g., [73, 74] and references therein).

Such "luminescent protection" works in a material, which has been investigated at the Institute of Physics for a long time – $BaMgAl_{l0}O_{17}$ (BAM) with a β-alumina structure (see, e.g., [75]). An impurity heavy (atomic mass 157) Eu^{2+} substitute for heavy Ba ions (152) located at an intermediate layer between two spinel blocks. It is important (see the text below), that Eu are spatially separated from each other even in the case of a high impurity concentration. The luminescence efficiency of such single impurity centers is high at the excitation by an electron beam or VUV-radiation of gas discharge. In addition, phosphor is sufficiently resistant against radiation.

It has long been known that doping of WGW with some heavy impurity ions (e.g. $Y_3Al_5O_{12}:Nd^{3+}$) leads to a sharp enhancement of material resistance against irradiation. During irradiation, Nd^{3+} impurity ions absorb a significant part of energy transforming it into infrared luminescence in the region of matrix transparency. Such transformation of the energy into luminescence leaving the sample can be considered as an efficient luminescent protection against radiation damage. $Y_3Al_5O_{12}:Nd^{3+}$ is known as an extremely powerful and resistant neodymium laser. Unfortunately, such effect is not valid for the emission of Ce^{3+} impurity ions introduced into YAG or LuAG.

There is some experimental evidences of a partial suppression of radiation damage in single crystals of lutetium-aluminum garnet lightly doped with Ce^{3+}. Figure 17 shows the spectra of radiation-induced absorption measured at RT after isodose irradiation of nominally pure LuAG and the crystal containing ~1400 ppm of Ce^{3+} ions with swift ^{197}Au ions (2.04 GeV, 10^{12} Au/cm^2, RT). In LuAG:Ce^{3+}, RIOA in the region of 5.2–6.1 eV is significantly lower. The analysis of these spectra shows that the presence of Ce^{3+} ions causes some decrease of RIOA connected with F-type centers. So, cerium ions prevent to some extent the creation of F-type centers by SHI. In the materials with $E_{FD} > E_g$, only recombination of hot conduction electrons with holes provides a sufficient energy for the creation of FD (see, e.g., [70]). In the presence of Ce^{3+}, hot electrons can

also excite Ce^{3+} ions resulting in an impurity luminescence. In our case, Ce^{3+} centers (in the case of relatively low concentration) in LuAG can be considered as luminescent protection against nonimpact mechanisms of radiation damage.
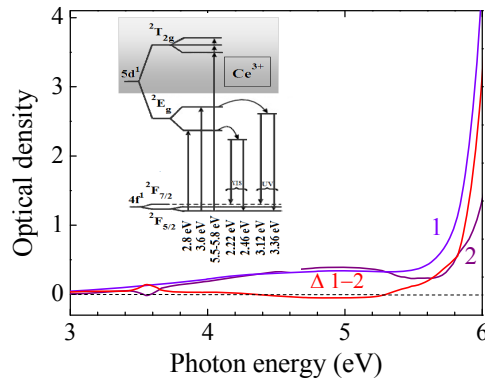

Figure 17. The spectra of radiation-induced optical absorption measured at 295 K after isodose irradiation of nominally pure LuAG (curve 1) or the crystal containing about 1400 ppm of Ce^{3+} impurity ions (LuAG:Ce, curve 2) with swift ^{198}Au ions (2.04 GeV, 10^{12} Au/cm^2, RT). Red curve shows the difference between curves 1 and 2. Inset shows the energy diagram for Ce^{3+} impurity ions in LuAG (see [76, 77] and references therein).

It is worth noting that one can expect a pronounced "luminescent protection" (i.e. decrease in the number of radiation-induced defects) at a sufficiently high cerium concentration (~1−2%). Unfortunately, according to the analysis of our experimental data, the situation at a high Ce^{3+} concentration becomes more complicated and can even cause the attenuation of LuAG radiation resistance due to some additional effects, which will be considered below.

Important results on irregular Ce^{3+} ions in LuAG:Ce^{3+} single crystals were presented in [78]. Based on a comparison of the EPR spectra related to Ce^{3+} in LuAG doped with two different cerium concentrations (8 and 550 ppm), it was stated that in addition to usual Ce^{3+} substituting for Lu^{3+} ($Ce|_{Lu}$), there also exists the so−called impurity antisite defect − a cerium ion, located in an octahedral Al^{3+} site, $Ce|_{Al}$. Because of the larger ionic radius of Ce^{3+} ion as compared with Lu^{3+} ion, $Ce|_{Al}$ causes a larger distortion of a crystal lattice as compared with the usual AD, $Lu|_{Al}$. The formation of $Ce|_{Al}$ is even more favourable near an anion vacancy (v_a or $v_a e$). So, single impurity AD as well as $Ce|_{Al}$ near to the F-type defects were revealed in LuAG single crystals using the EPR method.

The emission spectra of SHI-irradiated LuAG:Ce (1400 ppm) contain an emission band peaked at ~3.2 eV (see Fig. 18). The spectra were measured for a time-integrated signal or using two time-windows and at the excitation by 6.1

eV photons at 10 K. Fast emission of F^+ centers is not registered even in a short window. The emission at 3.1−3.4 eV can be connected with "an impurity anti-site defect" − Ce^{3+} ion located at an octahedral Al site. Earlier such $Ce|_{Al}$ in LuAG were detected and thoroughly investigated by the EPR and optical methods in [78]. A similar emission band was also detected in doped $\alpha-Al_2O_3$ for Ce^{3+} in an octahedral coordination (see, e.g., [23] and references therein).
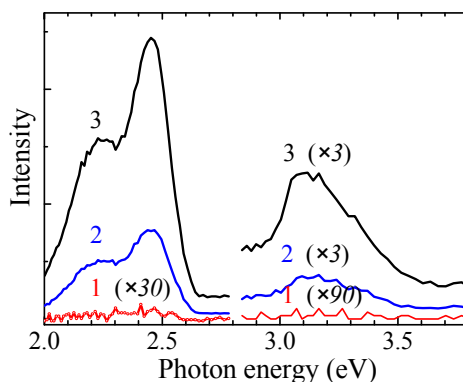

Figure 18. Emission spectra for a SHI-irradiated (^{197}Au) LuAG:Ce^{3+} (1400 ppm) crystal measured at the excitation by 6.1 eV photons at 10 K. The spectra are measured for different time windows (curve 1 – δt = 3 ns; Δt = 5 ns; curve 2 – δt = 20 ns; Δt = 30 ns) or for a time-integrated signal (curve 3) at 10 K.

So, Ce^{3+} impurity ions are mainly located at Lu^{3+}-sites ($Ce|_{Lu}$), but in the case of a high impurity concentration (or after SHI irradiation), there can also arise impurity antisite defects − Ce^{3+} ions substituting for Al^{3+} ions in octahedral positions. The increased number of impurity antisite defects can cause the decrease in the radiation resistance of LuAG. In a pair of spatially close heavy cerium ions, one of which substitute for light aluminum − $Ce|_{Al}$ and another is located in a regular Lu position ($Ce|_{Lu}$), there arises a strong local anharmonicity and such impurity pair can serve as a place for a collapse of supersonic discrete breathers resulting in the creation of temperature-stable 3D defects under high-dense irradiation (LET> 20 keV/nm). In such quasi-molecular complex, the distance between two Ce^{3+} ions is about a half of the distance between regular Lu sites in a crystal lattice (approximately 3 and 6 Å, respectively). As in this complex two large Ce ions would sit together, it seems reasonable, that somewhere in their vicinity an oxygen vacancy could be located to compensate for the space deficit.
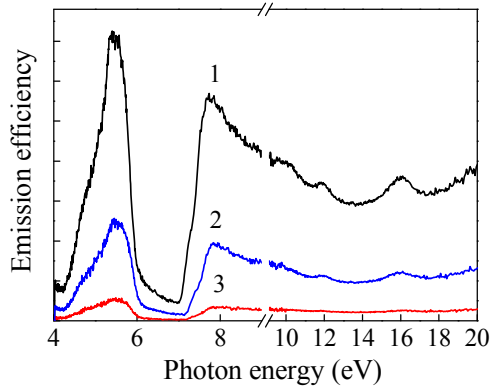
Figure 19. Excitation spectra for Ce^{3+} (2.46 eV) emission in LuAG:Ce (1400 ppm) irradiated by ^{197}Au ions (2.14 GeV, 10^{12} ions/cm^2, 295 K) at 10 K. The spectra are measured for time-integrated signal (curve 1) and two time windows (curve 2 – ($\delta t = 20$ ns; $\Delta t = 30$ ns), curve 3 – ($\delta t = 3$ ns; $\Delta t = 5$ ns).

Fig. 19 presents the excitation spectra measured for the 2.44 eV emission of single Ce^{3+} centers in SHI-irradiated $Lu_3Al_5O_{12}:Ce^{3+}$ (1400 ppm) using SR of 4–34 eV at 10 K. The spectra were measured under conditions of strong concentration quenching for a time-integrated (TI) luminescence as well as for the emission detected within short and long time windows (length Δt of 5 ns or 30 ns delayed with respect to the arrival of SR pulse by δt of 3 or 20 ns, respectively).
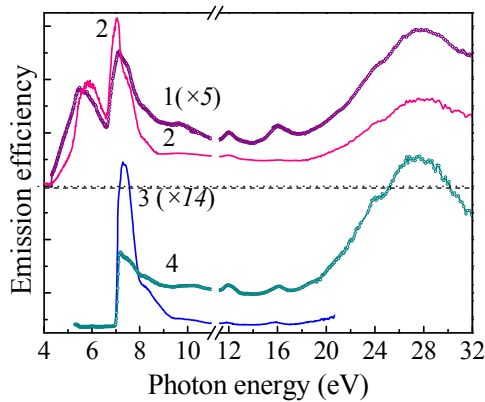

Figure 20. Excitation spectra of Ce^{3+} (2.44 eV) emission in LuAG:Ce (1400 ppm, curve 1) or LuAG:Ce (700 ppm, curve 2) at 10 K. Excitation spectra for 5.25 eV (self-trapped exciton, curve 3) or 4.75 eV (4) emission in nominally pure LuAG (~30 ppm of Ce^{3+}).

40

Fig. 20 presents the excitation spectra measured for the 2.44 eV emission of single Ce^{3+} centers in $Lu_3Al_5O_{12}:Ce^{3+}$ (1400 ppm) and $Lu_3Al_5O_{12}:Ce^{3+}$ (700 ppm) using SR of 4–34 eV at 10 K. At high cerium concentration (1400 ppm), the emission efficiency is significantly decreased (as compared to the case of 700 ppm – by ~5 times) because, in our opinion, the amount of complex cerium centers in the sample considerably exceeds the concentration of single Ce^{3+} centers typical of optimised scintillation detectors. The excitation spectra measured for two different Ce^{3+} concentrations considerably differ in the spectral region of $h\nu < 8.2$ eV.

In the region of fundamental absorption, the efficiency of cerium emission sharply increases at $h\nu > 19$ eV (see Fig. 20) due to the multiplication of electronic excitations, when an exciting photon forms two or even more excitations (two e–h pairs, e–h and anion exciton, etc.). Earlier this phenomenon was revealed and thoroughly studied in wide-gap materials of different types (see, e.g., [6, 68, 79, 80] and references therein). In the high-energy region, the efficiency is also high for the emission of self-trapped excitons (~5.2 eV), host anti-site defects $Lu|_{Al}$ (4.5 eV, see Fig. 20) and more complex defects with an emission at 3–4 eV. The excitation of complex metal oxides with photons of $h\nu > (2-3)E_g$ leads to a high local density of intrinsic electronic excitations due to the multiplication process. The presence of heavy rare-earth ions complicates the situation even more. A detailed consideration of these complicated processes still lies ahead.
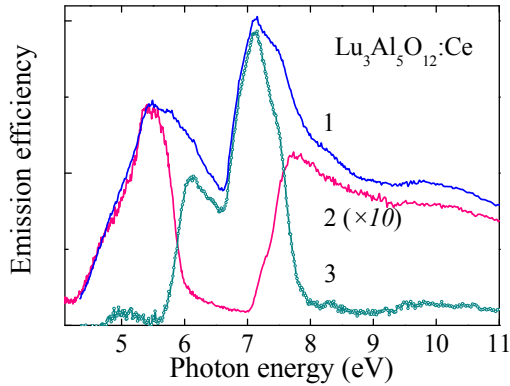

Figure 21. Excitation spectra for Ce^{3+} (2.46 eV) emission in virgin (1) and ^{197}Au irradiated (2) LuAG:Ce (1400 ppm) crystals, normalized to the low-energy band. The difference between curves 1 and 2 is given by line (3). Curve 2 is multiplied by a factor of 10.

41

In Section 3.2, the creation of radiation defects was registered via the comparison of the absorption and reflection spectra measured for virgin and SHI-irradiated LuAG single crystals. The excitation spectra for the emission of F, F^+ and AD were measured as well. It is worth noting that the appearance of radiation damage in SHI-irradiated crystals can be demonstrated even at a comparison of the excitation spectra measured for the Ce^{3+} emission (2.46 eV) in virgin and SHI-irradiated LuAG:Ce (1400 ppm) using SR at 10 K (see Fig. 21). The spectra are normalized at the low-energy maximum (curve for the irradiated sample is multiplied by ~10). An especially strong attenuation of Ce-emission efficiency takes place at 5.7–7.8 eV (see the difference curve in the figure). Radiation-induced defects are responsible for the increased absorption in this spectral regions: F-type defects at ~6.1 eV and intrinsic AD ($Lu|_{Al}$) at ~7.1 eV.

LuAG and GSO single crystals and optical ceramics with a complex crystal structure and optimal concentration of trivalent cerium ions (0.1–0.3 at%, ~1000 ppm) are widely used for technical applications. Ce^{3+} ions substitute for Lu^{3+} or Gd^{3+} ions with smaller ion radii (the Ce-radius is larger by 14 or 8%, respectively). At a higher impurity concentration, there occurs a sharp concentration quenching of luminescence. Such quenching is usually interpreted via dipole-dipole interaction of single Ce^{3+} centers causing migration of excited states along impurity centers in a crystal lattice and non-radiative decay of impurity excitations at surface, linear or other defects.

In our opinion, another interpretation, based on investigation of WGM with simple structure, can be considered as well. Besides single impurity centers, pair and more complex impurity centers with different optical characteristics appear in WGM with a sufficiently high impurity concentration. The formation of pair (two-impurity) centers in ionic-covalent WGM starts at a lower impurity concentration than it is typical of ionic crystals. This statement was demonstrated, for instance, by a comparative study of an ionic KCl:Tl crystal and KI:Tl with an enhanced level of covalency [81]. So, the presence of pair impurity ions should be definitely taken into consideration when investigating WGM with ionic-covalent binding.

Of particular interest is the presence of pairs of heavy impurity ions, one of which substitutes a light matrix ion in a crystal lattice. Such situation should cause a sharp quenching of impurity luminescence. Doping of WGM, built-up of light matrix ions, with even 1 at% of heavy rare-earth impurity ions leads to a significant decrease of the radiation resistance. Such enhancement of radiation damage is nicely expressed under high and superhigh density of radiation-induced excitations.

Fig. 10 in Section 3.2 demonstrated the emission spectra measured at the excitation of virgin and ion-irradiated LuAG:Ce (30 ppm) crystals by single electron pulses. The enhancement of the emission peak amplitude in the irradiated sample was detected only at 3.25–4.25 eV due to its short decay time (~70 ns) at 80 K. The emission undergoes thermal quenching already at 125 K. If the opposite, nonirradiated surface of LuAG (thickness ~1 mm) was excited by electron pulses, there was no ~3.75 eV emission at all. In our opinion, this

emission can be tentatively attributed to the pairs of Ce^{3+} ions, one of which is located at an octahedral Lu site and another – substitutes for a light Al^{3+} ("impurity AD"). $Ce|_{Al}$ causes a strong local anharmonicity (disbalance of masses by 5 times!) and pair cerium centers can serve as places for the collapse of the breathers resulting in a 3D defect creation under high-dense irradiation.

And finally some remarks, which, in our opinion, should be taken into account at the elaboration of novel WGM with a high light yield and acceptable radiation resistance. Based on long-standing experience in wide-gap luminescent materials for different applications, it is possible to conclude that these two properties are combined only in the doped materials, where not only valence and ion radius but also an atom mass are close for all elements of solid solution. For example, $CsI:Tl^+$, $LaBr_3:Ce^{3+}$ and $SrBr_2:Eu^{2+}$ fulfil all these requirements. In $LiI:Eu^{2+}$, $LaCl_3:Ce^{3+}$, $CaSO:Tb^{3+},F^-$ both light yield and radiation resistance are low even at a low impurity concentration. Especially harmful is the presence of the pairs of spatially close heavy rare-earth impurity ions. Even at the direct photoexcitation of these heavy pair-centers luminescence efficiency is low due to nonradiative transitions with a heat release. Mass disbalance results in the appearance of discrete breathers, the collapse of which under the conditions of high and superhigh excitation density occurs at pair-impurity centers and leads to the creation of complex defects. 3D defects serve as stoppers for dislocations and cause a cracking of single crystals. Optical ceramics and layered materials possess a higher radiation resistance, because dislocations can reach internal surfaces.

It can be tentatively mentioned, that if a pair consists of heavy but different impurity ions (for instance, Ce^{3+} and Tb^{3+}), the formation of an unified complex molecule is unlikely and a material is more resistant against radiation as compared to the presence of pairs identical rare-earth ions.

SUMMARY

The main investigation objects were binary (Al_2O_3) and complex ($Lu_3Al_5O_{12}$, Gd_2SiO_5) metal oxides with an increasing complicity of lattice and electronic structure as well as with a particular behavior of valence holes and excitons. The oxide crystals have a relatively high resistance against radiation (especially against the low-dense one with LET < 1 keV/nm) because the formation energy of a pair of Frenkel defects significantly exceeds the energy gap ($E_{FD} > E_g$) and the nonimpact creation mechanisms of Frenkel defects typical of alkali halides (the decay of self-trapping excitons or the recombination of relaxed conduction electrons with the self-trapped holes) are inefficient in these materials. A complex study of the creation processes of FD, their stable associations as well as extended and nanosize 3D defects (which determine a level of radiation resistance of these materials) by swift heavy ions providing a superhigh excitation density (^{197}Au, ^{238}U, ~2 GeV, 10^{11}–10^{13} ions/cm^2, range of 40–100 μm, LET > 20 keV/nm) has been performed. A comparative spectroscopic study of virgin and ion-irradiated metal oxides has been carried out using 4–40-eV photons, x-rays (~50 keV) and electrons (4–20 keV; 300 keV) in a wide temperature region (6–1425 K). Particular attention has been given to the contribution of single and pair impurity ions to the efficiency of radiation damage in metal oxides. The main results on the creation mechanisms of FD and nanosize 3D radiation defects and the prospects of their attenuation in some wide-gap dielectrics are the following:

1. Among the investigated nominally pure and doped (10^{-2}–10^{-4}) binary and complex metal oxides, pure (impurity level of $\leq 10^{-5}$) and stoichiometric MgO single crystals demonstrate the highest resistance against SHI-irradiation and sustain a fluence of 2×10^{13} ions/cm^2, while a cracking of complex oxides, containing heavy Lu^{3+} or Gd^{3+} cations and many atoms per unit cell, occurs already at $\Phi = 2 \times 10^{12}$ ions/cm^2, when the average distance between the centers of the neighboring track is about 7 nm. It is shown, that besides the universal knock-out mechanism connected with elastic collisions of incident SHI with the atoms (nuclei) of a crystal, some novel nonimpact mechanisms (e.g., hot e–h recombination) are responsible for the creation of FD and their elementary associations at the periphery of ion tracks in irradiated ($\Phi = 10^{11}$–10^{12} ions/cm^2) nominally pure Al_2O_3, $Lu_3Al_5O_{12}$ and Gd_2SiO_5 single crystals. There are certain differences in the radiation damage of Al_2O_3 induced by ~2-GeV SHI, which spend more than 99% of their energy on ionization losses, or fast neutrons, when the knock-out mechanism is a dominant one. In Al_2O_3, the majority of the ion-irradiation-induced F^+ and F centers partly created via recombination of non-relaxed conduction electrons with localized holes can be annealed by heating up to 900 K, while the decrease of still unidentified centers (absorption bands at 5.8–6.5 eV) occurs at higher temperatures.

2. Some experimental manifestations of the creation of nanosize 3D defects have been detected in $Lu_3Al_5O_{12}$ and, especially, Gd_2SiO_5 crystals irradiated

with swift heavy ions (~2 GeV, ^{197}Au or ^{238}U ions, fluence of 10^{12} ions/cm^2). 3D defects are temperature-stable, long-lived at RT and cause a significant rise of scattered light at $h\nu > 4$ eV in Gd_2SiO_5. Analysis of the annealing of radiation-induced optical absorption (measured using a double monochromator) showed that, contrary to the F and F$^+$ centers formed at the periphery of ion tracks, 3D defects are stable even at ~0.7T_m (limit of our preheating in a very dry atmosphere).

According to theoretical predictions [20], similar nanosize 3D intrinsic defects (~10−20 nm) are created in metal alloys via rearrangement of many host ions at the collapse of supersonic intrinsic discrete solitons formed under conditions of high dense irradiation. An intrinsic discrete mode with a large amplitude and frequency above the top of the acoustic phonon spectrum may exist at the dense excitation of crystals predisposed to anharmonic interactions [17−21]. These discrete breathers (also referred to as discrete solitons) should be especially strong in the materials built up of ions with very different masses (e.g., Gd_2SiO_5 and $Lu_3Al_5O_{12}$). In this case, the frequency of discrete supersonic breathers can fall in a gap between acoustic and optical vibration branches. Similar to metal alloys, in Gd_2SiO_5 irradiated with 2×10^{12} ions/cm^2, nanosize 3D defects serve as stoppers for dislocations, seeds for micro- and macro-cracks and facilitate brittle destruction of the crystal.

3. The analysis of the spectra of SHI-induced absorption of nominally pure or Ce-doped LuAG crystals shows some enhancement of radiation resistance (decrease in the number of radiation-induced F-type centers) of the doped sample. In LuAG with $E_{FD} > E_g$, only hot $e-h$ recombination provides the energy sufficient for the nonimpact creation of FD. However, hot conduction electrons can be cooled via the direct excitation of Ce^{3+} impurity ions resulting in impurity luminescence. The latter process − a solid-state analogue of the Franck-Hertz effect, is a luminescent dissipation channel for the energy absorbed by a crystal during irradiation that competes with the nonradiative channel of FD creation. The so-called "luminescent protection" against FD creation via hot $e-h$ recombination has been revealed for the first time in complex metal oxide single crystals doped with a relatively low impurity concentration, when single impurity centers are dominant.

However, the situation with radiation resistance becomes rather different with a rise of impurity concentration up to 1−2% that is needed for pronounced "luminescent protection." According to the analysis of our and literature experimental data, a high efficiency of radiation damage (and, respectively, decrease of the resistance against irradiation) is typical of complex divalent metal oxides, which contain pairs (spatially correlated) of heavy rare-earth impurity ions. Firstly, pair centers can serve as traps for radiation-induced holes, thus enhancing their recombination efficiency with hot conduction electrons (hot $e-h$ recombination). Secondly, in our opinion, the pairs of heavy impurity ions provide mass disbalance (at least one of impurity ions substitutes for a light matrix metal), anharmonicity of the system and favorable conditions for the

existence of discrete breathers. In $Lu_3Al_5O_{12}:Ce^{3+}$, a pair of two spatially close cerium ions, one of which substitute for lutetium and the another, for light aluminium (i.e., "impurity antisite defect") causes a strong local anharmonicity and can serve as a place for a collapse of discrete breathers with the creation of 3D defects under a high dense irradiation. According to our experience with super-high-dense irradiation of doped WGM, the well-known concentration quenching of heavy rare-earth impurity luminescence correlates with the decrease of radiation resistance of these materials.

KOKKUVÕTE

Struktuuridefektide teke laia keelupiluga metallioksiidides ülisuure kiiritustiheduse tingimustes

Põhilisteks uurimisobjektideks olid erineva võre ja elektronstruktuuri keerukuse ning valentstsooni aukude ja eksitonide käitumisega binaarsed (Al_2O_3) ja komplekssed ($Lu_3Al_5O_{12}$, Gd_2SiO_5) metallioksiidid. Oksiidi kristallide kiirituspüsivus on suhteliselt kõrge (eriti madala kiiritustiheduse korral, kui LET < 1 keV/nm), kuna Frenkeli paaride moodustumise energia on keelupilu laiusest oluliselt suurem ($E_{FD} > E_g$) ning leelishalogeniididele tüüpilised Frenkeli defektide tekke mittelöökmehhanismid (iselõksustunud eksitonide lagunemine või relakseerunud elektronide ning iselõksustunud aukude rekombinatsioon) ei ole neis materjalides efektiivsed. Antud töös on komplekssstelt uuritud Frenkeli defekte (FD), nende stabiilsete ühenduste, samuti nii ulatuslike kui nanomõõduliste 3D defektide (mis kõik määravad nende materjalide kiirituspüsivuse taset) tekkeprotsesse ülikõrget ergastustihedust põhjustavate kiirete raskete ioonidega (^{197}Au, ^{238}U, ~2 GeV, 10^{11}–10^{13} iooni/cm^2, kiiritamissügavus 40–100 µm, LET > 20 keV/nm) kiiritamisel. Kasutades 4–40 eV footoneid, ~50 keV röntgenkiirgust ning elektrone (4–20 eV, 300 keV) viidi laias temperatuurivahemikus (6–1425 K) läbi puutumatute ning ioon-kiiritatud metallioksiidide võrdlev spektroskoopiline uurimus. Erilise tähelepanuga uuriti üksikute lisandioonide ning nende paaride mõju metallioksiidide kiirituspüsivusele. FD ja nanomõõduliste 3D kiiritusdefektide tekkemehhanismide uurimise ning nende mõju leevendamise väljavaadete peamised tulemused mõnede laia keelupiluga dielektrikute jaoks on järgmised:

1. Uuritud nominaalselt puhaste ning legeeritud (10^{-2}–10^{-4}) binaarsete ning komplekssete metallioksiidide seas kõige vastupidavamad SHI kiirusele olid puhtad (lisandite tase $\leq 10^{-5}$) ning stöhhiomeetrilised MgO monokristallid, mis talusid kiiritust 2×10^{13} iooni/cm^2, samas kui raskeid Lu^{3+} või Gd^{3+} katioone sisaldavad ning ühikrakus palju aatomeid sisaldavad kompleksoksiidid pragunesid juba $\Phi = 2 \times 10^{12}$ ions/cm^2 juures, mil naabertrekkide vaheline keskmine vahekaugus oli ca 7 nm. Näidati, et lisaks universaalsele, pealelangevate SHI-de ning kristalli aatomite (tuumade) vaheliste elastsete põrgetega seotud põrkemehhanismile tekitavad kiiritatud ($\Phi = 10^{11}$–10^{12} ions/cm^2) nominaalselt puhaste Al_2O_3, $Lu_3Al_5O_{12}$, Gd_2SiO_5 monokristallide ioontrekkide perifeerias FD ja nende elementaarseid komplekse ka mõned uued mittepõrkemehhanismid (näit kuumad e–h rekombinatsioonid). On selged erinevused Al_2O_3 kiirtuskahjustustes, sõltuvalt sellest, kas neid on tekitatud ~2 GeV SHI-dega, mille energiast üle 99% kulub ionisatsioonikadudele, või kiirete neutronitega, mille korral domineerivad põrkeprotsessid. Enamikku Al_2O_3-s ioonkiiritamisel, neist osa relakseerumata juhtivuselektronide ja lokaliseerunud aukude rekombinatsiooni tulemusel, tekkinud F^+ ja F-tsentreist saab kõrvaldada, kuumutades kristalli 900 K-ni, samas seni identifitseerimata tsentrite (neeldumine 5,8-6,5 eV piirkonnas) arvu langus toimub kõrgemal temperatuuril.

2. Kiirete raskete ioonidega kiiritatud (~2 GeV, ^{197}Au või ^{238}U ioonid, voo tihedus 10^{12} iooni/cm^2) $Lu_3Al_5O_{12}$ ning eriti Gd_2SiO_5 kristallides jälgiti nano-mõõduliste 3D defektide teket. 3D defektid on toatemperatuuril (RT) tempera-tuuriliselt stabiilsed ning Gd_2SiO_5 -s põhjustavad olulist $hv > 4$ eV valguse haju-mise kasvu. Kiirituse poolt indutseeritud optilise neeldumise (mõõdetud topelt-monokromaatoriga) temperatuurilise kustumise analüüs näitas, et, erinevalt iooni trekkide perifeerias moodustunud F ja F$^+$ -tsentritest, on 3D defektid stabiilsed isegi ~$0,7T_m$ juures (meie kuumutamise piir väga kuivas atmosfääris).

Vastavalt teoreetilistele ennustustele [20] tekivad sarnased nanomõõdulised (~10–20 nm) 3D omadefektid metallisulameis kõrge kiiritustiheduse tingimus-tes moodustunud ülihelikiiruslike diskreetsete solitonide kollapsi korral, mis põhjustab paljude põhiaine ioonide ümberpaiknemist. Suure amplituudiga ning akustilise foononspektri kohal paikneva kõrge sagedusega diskreetne mood võib kõrge ergastuse korral aset leida kristallides, millele on omased anharmoonili-sed vastasmõjud [17–21]. Need diskreetsed *breather*'id (ehk diskreetsed solito-nid) peaksid olema eriti tugevad materjalides, mis koosnevad väga erineva mas-siga ioonidest (näit Gd_2SiO_5 ja $Lu_3Al_5O_{12}$). Sel juhul diskreetsete ülihelikiirus-like *breather*'ite sagedus võib sattuda akustiliste ja optiliste võnkumiste vahe-lisse lõhesse. Sarnaselt metallisulameile, 2×10^{12} ioons/cm^2 kiiritatud Gd_2SiO_5-s nanomõõtmelised 3D defektid takistavad dislokatsioonide liikumist, on seem-neks mikro- ja makropragudele ning hõlbustavad kristalli purunemist.

3. Nominaalselt puhaste ning Ce^{3+} legeeritud LuAG kristallide SHI-indut-seeritud neeldumisspektrite analüüs näitas legeeritud objektide kiirituspüsivuse mõningat paranemist (kiiritamisel tekkinud F-tüüpi tsentrite arvu kahanemist). LuAG-s, mille $E_{FD} > E_g$, ainult kuumad *e–h* rekombinatsioonid vabastavad piisavalt energiat tekitamaks FD mittelöökmehhanismi teel. Kuid kuumi elekt-rone saab jahutada, kui nad vahetult ergastavad Ce^{3+} lisandioone koos järgneva lisandluminestsentsiga. See viimane protsess – Franck-Hertz'i efekti analoog tahkises – kujutab endast luminestsentset kanalit kiiritamisel kristallis neeldu-nud energia hajutamiseks, mis konkureerib mittekiirgusliku FD tekitamise kana-liga. See nn luminestsentsikaitse *e–h* rekombinatsioonide vahendusel toimuvate FD tekitamise vastu tuvastati esmakordselt suhteliselt madala lisandi kontsent-ratsiooniga komplekssetes metallioksiidide monokristallides, kus domineerivad isoleeritud lisanditsentrid.

Kiirituspüsivuse olukord muutub aga oluliselt, kui lisandi kontsentratsioon kasvab 1–2%-ni, mis on mõjusaks luminestsentsikaitseks vajalik. Vastavalt meie ning kirjandusest leitud eksperimentaalandmete analüüsile, kiirituskahjus-tuse kõrge efektiivsus (ning vastavalt kiirituskindluse langus) on tüüpiline komplekssetele kahevalentsetele metallioksiididele, mis sisaldavad raskete muldmetalli lisandioonide (ruumiliselt korreleeritud) paare. Esiteks, paaris-tsentrid võivad haarata kiiritamisel tekkinud auke, suurendades seeläbi nende kuumade juhtivuselektronidega rekombineerumise tõenäosust (kuumad *e–h* re-kombinatsioonid). Teiseks, meie arvates tekitavad raskete lisandioonide paarid massi disbalansi (vähemalt üks lisandioon asendab kerge põhiaine iooni), süs-teemi anharmoonilisuse ning soodsad tingimused diskreetsete *breather*'ite

tekkeks. $Lu_3Al_5O_{12}:Ce^{3+}$-s ruumiliselt lähedaste tseeriumi ioonide paar, millest üks asendab luteetsiumi ning teine kerge alumiiniumi (s.t vastandpositsiooniga lisanddefekt) põhjustab tugevat lokaalset anharmonismi ning võib olla kohaks, kus kõrge kiiritustiheduse tingimustes diskreetsete *breather*'ite kollapsil tekivad 3D defektid. Meie ülikõrge tihedusega kiiritatud legeeritud laia keelupiluga materjalide kohta käiva kogemuse põhjal hästi tuntud raskete muldmetalli li-sandioonide luminestsentsi kustumine korreleerub kiirituspüsivuse langusega neis materjalides.

REFERENCES

[1] M. Thompson, *Defects and Radiation Damage in Metals* (Univ. Press, Cambridge, 1969). (М. Томпсон, Дефекты и радиационные повреждения в металлах, М.: Мир, 1971)

[2] *Radiation Effects in Solids,* ed. by K. E. Sickafus, E. A. Kotomin, and B. P. Uberuaga, (Springer, Amsterdam, 2007)

[3] G. A. Malygin, Phys. Usp. **54**, 1091−1116 (2011)

[4] N. Itoh and A. M. Stoneham, *Material Modification by Electronic Excitation*, (Univ. Press, Cambridge. 2000)

[5] Ch. B. Lushchik, I. K. Vitol, M. A. Elango, *Usp. Fiz. Nauk* **122**, 223–251 (1977)

[6] Ch. B. Lushchik and A. Ch. Lushchik, Decay of Electronic Excitations with Defect Formation in Solids. Nauka, Moscow (1989). (Ч. Б. Лущик, А. Ч. Лущик, Распад электронных возбуждений с образованием дефектов в твёрдых телах, М.: Наука, 1989)

[7] K. S. Song and R. T. Williams, *Self-Trapped Excitons*. Second Edition. (Springer, Berlin, 1996).

[8] A. Lushchik, Ch. Lushchik, T. Kärner, V. Nagirnyi, E. Shablonin, E. Vasil'chenko, *Izv. VUZOV. Fizika (Russian Physics Journal)* **52**, 95–100 (2009)

[9] E. Feldbach, A. Lushchik, Ch. Lushchik, V. Nagirnyi, E. Shablonin, and S. Vielhauer, in: MAX-lab Activity Report 2010 (National Laboratory, Lund, Sweden 2010) pp. 462-463.

[10] A. Ch. Lushchik and Ch. B. Lushchik, *Bull. Russ. Acad. Sci. Phys.* **56**, 201–206 (1992)

[11] D. I. Vaisburd and I. N. Balychev, *Sov. Phys. JETP* **15**, 380−383 (1972).

[12] Д. И. Вайсбурд, Б. Н. Семин, Э.Г. Таванов, С. Ф. Матлис, И. Н. Геринг, *Высокоэнергетическая электроника твёрдого тела*, Новосибирск: Наука, 1982

[13] D. I. Vaisburd and K. E. Evdokimov, *Phys. Status Solidi* C, 216−222 (2005)

[14] E. Balanzat, S. Bouffard, A. Cassimi, E. Dooryhee, J. P. Grandin, J. L. Doualan, J. Margerie, *Nucl. Instrum. Methods* B **91**, 134−139 (1994)

[15] K. Schwartz, C. Trautmann, A. S. El-Said, R. Neumann, M. Toulemonde, W. Knolle, *Phys. Rev.* B **70**, 184104 (2004)

[16] K. Schwartz, A. E. Volkov, K.-O. Voss, M. V. Sorokin, C. Trautmann, R. Neumann, *Nucl. Instrum. Methods* B **245**, 204–209 (2006)

[17] S. A. Kiselev and A. J. Sievers, *Phys. Rev.* B **55**, 5755−5758 (1997)

[18] M. Haas, V. Hizhnyakov, A. Shelkan, M. Klopov, and A. J. Sievers, *Phys. Rev. B* **84**, 144303 (2011)

[19] H. Guo, M. Zhang, J. Han, H. Zhang, N. Song, *Physica* B **407**, 2262−2266 (2012)

[20] V. E. Zakharov and E. A. Kuznetsov, *Phys. Usp.* **55**, 535−556 (2012)

[21] J. F. Ziegler, J. P. Biersack, and U. Littmark, in *The Stopping and Ranges of Ions in Solids*, ed. by J. F. Ziegler (Pergamon, New York, 1985), pp. 308-315.

[22] G. Zimmerer, *Rad. Meas.* **42**, 859−864 (2007)

[23] L. M. Belyaev (ed), *Ruby and Sapphire* (Nauka, Moscow, 1974). (Рубин и Сапфир, М.: Наука, 1974)

[24] *Препаративные методы в химии твердого тела*, под ред. П. Хагенмюллера (Мир, Москва, 1976) стр. 188

[25] Б. Х. Намозов, *Электронные возбуждения и коротковолновая люминесценция кристаллов* Al_2O_3, $YAlO_3$, $Y_3Al_5O_{12}$. Диссерт. канд. ф.-м.н., наук, Тарту 1987

[26] F. Euler and J. A. Bruce, *Acta Crystallogr.* **19**, 971−978 (1965)

[27] M. Nikl, V. V. Laguta, A. Vedda, *Phys. Status Solidi* B **245**, 1701−1722 (2008)

[28] Y. Zorenko, V. Gorbenko, E. Mihokova, M. Nikl, K. Nejezchle, A. Vedda, V. Kolobanov, D. Spassky, *Radiat. Meas.* **42**, 521−527 (2007)

[29] K. Blazek, A. Krasnikov, K. Nejezchleb, M. Nikl, T. Savikhina, S. Zazubovich, *Phys. Status Solidi* B **241,** 1134−1140 (2004)

[30] Y. Zorenko, T. Zorenko, V. Gorbenko, B. Pavlyka, V. Laguta, M. Nikl, V. Kolobanov, D. Spassky, *Radiat. Meas.* **45**, 409−421 (2010)

[31] Yu. Zorenko, A. Voloshinovskii, V. Savchyn, T. Vozniak, M. Nikl, K. Nejezchleb, V. Mikhailin, V. Kolobanov, D. Spassky, *Phys. Status Solidi* B **244**, 2180−2189 (2007)

[32] T. Gustafsson, M. Klintenberg, S. E. Derenzo, M. J. Weber, J. O. Thomas, *Acta Crystallogr.* C **57**, 668−669 (2001)

[33] I. Gerasymov, O. Sidletskiy, S. Neicheva, B. Grinyov, V. Baumer, E. Galenin, K. Katrunov, S. Tkachenko, O. Voloshina, A. Zhukov, Growth of bulk gadolinium pyrosilicate single crystals for scintillators, *J. Cryst. Growth* **318**, 805–808, (2011)

[34] V. Bondar, B. Grinyov, K. Katrunov, L. Lisetski, L. Nagornaya, V. Ryzhikov, V. Spasov, N. Starzhinskiy, G. Tamulaitis, *Nucl. Instrum. Methods* A **537**, 215–218 (2005).

[35] O. Sidletskiy, V. Baumer, I. Gerasymov, B. Grinyov, K. Katrunov, N. Starzhinsky, O. Tarasenko, V. Tarasov, S. Tkachenko, *Radiat. Meas.* **45**, 365–368 (2010)

[36] S.-D. Mo and W. Y. Ching, *Phys. Rev.* B **57**, 15219−15228 (1998)

[37] Y.-N. Xu and W. Y. Ching, *Phys. Rev.* B **59**, 10530−10535 (1999)

[38] W. Setyawan, R. M. Gaumé, R. S. Feigelson, S. Curtarolo, *IEEE Trans. Nucl. Sci.* **56**, 2989−2996 (2009)

[39] M. Kirm, G. Zimmerer E. Feldbach, A. Lushchik, Ch. Lushchik, F. Savikhin, *Phys. Rev.* B **60**, 502−510 (1999)

[40] W. Y. Ching, and Y.-N. Xu, J. Amer. Soc. 77, 404−411 (1994)

[41] M. Kirm, E. Feldbach, A. Kotlov, P. Liblik, A. Lushchik, M. Oja, E. Palcevskis, *Radiat. Meas.* **45**, 618−620 (2010)

[42] A. I. Kuznetsov, V. N. Abramov, V. V. Mürk, B. R. Namozov, *Trudy Instituta Fiziki EstSSR* **63**, 19–42 (1982)

[43] V. Mürk, A. Kuznetsov, B. Namozov, K. Ismailov. Relaxation of electronic excitations in YAG and YAP crystals. *Nucl. Instrum. Methods* B **91**, 327–330 (1994)

[44] V. Babin, V. Bichevin, V. Gorbenko, M. Kink, A. Makhov, Yu. Maksimov, M. Nikl, G. Stryganyuk, S. Zazubovich, Yu. Zorenko, *Phys. Status Solidi* B **248**, 1505−1512 (2011)

[45] M. Nikl, A. Vedda, M. Fasoli, I. Fontana, V. V. Laguta, E. Mihokova, J. Pejchal, J. Rosa, K. Nejezchleb, *Phys. Rev.* B **76**, 195121 (2007)

[46] P. Dorenbos, *J. Lumin.* **134**, 310–318 (2013)

[47] R. I. Eglitis, E. A. Kotomin, G. Borstel, *J. Phys.: Condens. Matter* **14**, 3775−3741 (2002).

[48] O. F. Schirmer, *J. Phys.: Condens. Matte*r **18**, R667−R704 (2006).

[49] A. M. Stoneham, J. Gavartin, A. L. Shluger, A. V. Kimmel, D. Munoz Ramo, G. Aeppli, C. Renner, *J. Phys.: Condens. Matter* **19**, 255208 (2007)

[50] M. Kirm, G. Stryganyuk, S. Vielhauer, G. Zimmerer, V. N. Makhov, B. Z. Malkin, O. V. Solovyev, R. Yu. Abdulsabirov, S. L. Korableva, *Phys. Rev.* B **75**, 075111 (2007)

[51] V. Babin, V. V. Laguta, A. Maaroos, A. Makhov, M. Nikl, S. Zazubovich, *Phys. Status Solidi* B **248**, 239–242 (2011)

[52] M. M. Kuklja. *J. Phys.: Condens. Matter* **12**, 2953−2967 (2000)

[53] B. D. Evans and M. Stapelbroek, *Phys. Rev.* B **18**, 7089−7098 (1978)

[54] I. I. Milman, V. S. Kortov, S. V. Nikiforof, *Radiat. Meas*. **29**, 401−410 (1998)

[55] J.M. Bunch, F.W. Clinard, *J. Amer. Ceram. Soc.* **57**, 279−280 (1974)

[56] K.H. Lee, J.H. Crawford, *Phys. Rev.* B **15**, 4065−4070 (1977)

[57] A. Lushchik, Ch. Lushchik, K. Schwartz, E. Vasil'chenko, R. Papaleo, V. Sorokin, A. E. Volkov, R. Neumann, C. Trautmann, *Phys. Rev.* B **76**, 054114 (2007)

[58] A. R. Silins and A. N. Trukhin, Point Defects and Elementary Excitations in Crystalline and Glass SiO$_2$ (Zinatne, Riga, 1985)

[59] L. Skuja, M. Hirano, H. Hosono, K. Kajihara, *Phys. Status Solidi* C **2**, 15−24 (2005)

[60] V. Yu. Ivanov, E. S. Slygin, V. A. Pustovarov, V. V. Mazurenko, B. V. Shulgin, *Phys. Solid State* **50**, 1692−1698 (2008)

[61] V. Yu. Ivanov, A. V. Kruzhalov, M. Kobayashi, E. S. Slygin, V. A. Pustovarov, B. V. Shulgin, *Phys. Procedia* **2**, 349−352 (2009)

[62] D. W. Cooke, B. L. Bennett, K. J. McClellan, J. M. Roper, M. T. Whittaker, *J. Lumin*. **92**, 83−89 (2001)

[63] B. Toxanbayev, E. Vasil'chenko, A. Zhunusbekov, A. Lushchik, V. Nagirnyi, T. Nurakhmetov, F. Savikhin, *Bull. Nat. Acad. Sci. Rep. Kazakhstan*, **3**, 10−13 (2009).

[64] A. A. O'Connel-Bronin, Sov. *Phys. Solid State* **26**, 2603−2610 (1984)

[65] M. E. Manley, A. J. Sievers, J. W. Lynn, S. A. Kiselev, S. A. Agladze, Y. Chen, A. Llobet, A. Alatas, *Phys. Rev*. B **79**, 134304 (2009)

[66] H. Bilz and W. Kress, *Phonon Dispersion Relations in Insulators* (Springer, Berlin, 1979)

[67] K. Kimura, S. Sharma, A. I. Popov, *Radiat. Meas*. **34**, 99−103 (2001)

[68] E. Feldbach, M. Kamada, M. Kirm, A. Lushchik, Ch. Lushchik, I. Martinson, *Phys. Rev.* B **56**, 13908−13915 (1997)

[69] A. Lushchik, M. Kamada, M. Kirm, Ch. Lushchik, I. Martinson, *Radiat. Meas*. **29**, 229−234 (1998)

[70] A. Lushchik, Ch. Lushchik, M. Kirm, V. Nagirnyi, F. Savikhin, E. Vasil'chenko, *Nucl. Instrum. Methods B* **250**, 330–336 (2006)

[71] A. Lushchik, Ch. Lushchik, P. Liblik, A. Maaroos, V.N. Makhov, F. Savikhin, E. Vasil'chenko. *J. Lumin*. **129**, 1894−1897 (2009)

[72] V. N. Makhov, A. Lushchik, Ch. B. Lushchik, M. Kirm, E. Vasil'chenko, S. Vielhauer, V. V. Harutunyan, E. Aleksanyan, *Nucl. Instrum. Methods* B **266**, 2949−2952 (2008)

[73] A. I. Popov, E. A. Kotomin, J. Majer, Nucl. *Nucl. Instrum. Methods* B, **268** 3084−3089 (2010)

[74] E. A. Kotomin and A. I. Popov, in *Radiation Effects in Solids,* eds. K. E. Sickafus, E. A. Kotomin, B. P. Uberuaga, (Springer, Amsterdam, 2007) Chapter 7

[75] A. Lushchik, Ch. Lushchik, E. Feldbach, I. Kudrjavtseva, P. Liblik, A. Maaroos, V. Nagirnyi, E. Vasil'chenko, F. Savikhin. *Proc. SPIE* **5946**, 594609 (2005)

[76] P. Dorenbos, *J. Lumin*. **99**, 283–299 (2002)

[77] V. Babin, V. Gorbenko, A. Makhov, J.A. Mares. M. Nikl, S. Zazubovich, Yu. Zorenko, , *J. Lumin*. **127**, 2, 384–390 (2007)

[78] V. Babin, V. V. Laguta, A. Makhov, K. Nejezchleb, M. Nikl, S. Zazubovich, *EEE Trans. Nucl. Sci*. **55**, 1156–1159 (2008)

[79] E. R. Ilmas and T. I. Savikhina, *J. Lumin*. **1–2**, 325–334 (1970)

[80] Ju. Aleksandrov, A. Kuznetsov, Ch. Lushchik, V. Makhov, I. Meriloo, T. Savikhina, T. Syreishchikova, M. Jakimenko, *Trudy Instituta Fiziki EstSSR* **53**, 7–30 (1982).

[81] T. Nurakhmetov and R. Gindina, *Trudy Instituta Fiziki i Astronomii EstSSR* **44**, 145–153 (1975).

AKNOWLEDGEMENTS

I would like to thank my supervisor Prof. Aleksandr Lushchik for guiding me during the years needed to complete this thesis.

CURRICULUM VITAE

Name: Anna Shugai
Date of birth: 11.03.1985
Citizenship: Estonia
Phone: 58251381
E-mail: annasu@ut.ee

Education:
1991–2003   Maardu Gymnasium
2003–2006   B.Sc, University of Tartu
2006–2008   M.Sc, University of Tartu
2008–2013   PhD studies, University of Tartu

Professional employment:
2011 – present University of Tartu, Institute of Physics, engineer

Language skills:
Russian, Estonian, English

Main field of research:
Solid state physics, optical properties and radiation resistance of wide-gap metal oxides

ELULOOKIRJELDUS

Nimi: Anna Shugai
Sünniaeg: 11.03.1985
Kodakondsus: Estonia
Telefon: 58251381
E-mail: annasu@ut.ee

Haridus:
1991−2003   Maardu Gümnaasium, keskharidus
2003−2006   Tartu Ülikool, Materjaliteaduse bakalaureuse kraad
2006−2008   Tartu Ülikool, Materjalitehnoloogia magistri kraad
2008−k.a.   Tartu Ülikool, Füüsika Doktoriõpe

Teenistuskäik:
2011 – k.a.   Tartu Ülikool, Füüsikainstituut, insener

Keelteoskus:
vene keel, eesti keel, inglise keel

Peamised uurimisvaldkonnad:
Tahke keha füüsika, laia piluga metalloksiidide optilised omadused ja kiiritus-kindlus

DISSERTATIONES PHYSICAE
UNIVERSITATIS TARTUENSIS

1. **Andrus Ausmees.** XUV-induced electron emission and electron-phonon interaction in alkali halides. Tartu, 1991.
2. **Heiki Sõnajalg.** Shaping and recalling of light pulses by optical elements based on spectral hole burning. Tartu, 1991.
3. **Sergei Savihhin.** Ultrafast dynamics of F-centers and bound excitons from picosecond spectroscopy data. Tartu, 1991.
4. **Ergo Nõmmiste.** Leelishalogeniidide röntgenelektronemissioon kiiritamisel footonitega energiaga 70–140 eV. Tartu, 1991.
5. **Margus Rätsep.** Spectral gratings and their relaxation in some low-temperature impurity-doped glasses and chrystals. Tartu, 1991.
6. **Tõnu Pullerits.** Primary energy transfer in photosynthesis. Model calculations. Tartu, 1991.
7. **Olev Saks.** Attoampri diapasoonis voolude mõõtmise füüsikalised alused. Tartu, 1991.
8. **Andres Virro.** AlGaAsSb/GaSb heterostructure injection lasers. Tartu, 1991.
9. **Hans Korge.** Investigation of negative point discharge in pure nitrogen at atmospheric pressure. Tartu, 1992.
10. **Jüri Maksimov.** Nonlinear generation of laser VUV radiation for high-resolution spectroscopy. Tartu, 1992.
11. **Mark Aizengendler.** Photostimulated transformation of aggregate defects and spectral hole burning in a neutron-irradiated sapphire. Tartu, 1992.
12. **Hele Siimon.** Atomic layer molecular beam epitaxy of A^2B^6 compounds described on the basis of kinetic equations model. Tartu, 1992.
13. **Tõnu Reinot.** The kinetics of polariton luminescence, energy transfer and relaxation in anthracene. Tartu, 1992.
14. **Toomas Rõõm.** Paramagnetic H^{2-} and F^+ centers in CaO crystals: spectra, relaxation and recombination luminescence. Tallinn, 1993.
15. **Erko Jalviste.** Laser spectroscopy of some jet-cooled organic molecules. Tartu, 1993.
16. **Alvo Aabloo.** Studies of crystalline celluloses using potential energy calculations. Tartu, 1994.
17. **Peeter Paris.** Initiation of corona pulses. Tartu, 1994.
18. **Павел Рубин.** Локальные дефектные состояния в CuO_2 плоскостях высокотемпературных сверхпроводников. Тарту, 1994.
19. **Olavi Ollikainen.** Applications of persistent spectral hole burning in ultrafast optical neural networks, time-resolved spectroscopy and holographic interferometry. Tartu, 1996.
20. **Ülo Mets.** Methodological aspects of fluorescence correlation spectroscopy. Tartu, 1996.
21. **Mikhail Danilkin.** Interaction of intrinsic and impurity defects in CaS:Eu luminophors. Tartu, 1997.

22. **Ирина Кудрявцева.** Создание и стабилизация дефектов в кристаллах KBr, KCl, RbCl при облучении ВУФ-радиацией. Тарту, 1997.

23. **Andres Osvet.** Photochromic properties of radiation-induced defects in diamond. Tartu, 1998.

24. **Jüri Örd.** Classical and quantum aspects of geodesic multiplication. Tartu, 1998.

25. **Priit Sarv.** High resolution solid-state NMR studies of zeolites. Tartu, 1998.

26. **Сергей Долгов.** Электронные возбуждения и дефектообразование в некоторых оксидах металлов. Тарту, 1998.

27. **Kaupo Kukli.** Atomic layer deposition of artificially structured dielectric materials. Tartu, 1999.

28. **Ivo Heinmaa.** Nuclear resonance studies of local structure in $RBa_2Cu_3O_{6+x}$ compounds. Tartu, 1999.

29. **Aleksander Shelkan.** Hole states in CuO_2 planes of high temperature superconducting materials. Tartu, 1999.

30. **Dmitri Nevedrov.** Nonlinear effects in quantum lattices. Tartu, 1999.

31. **Rein Ruus.** Collapse of 3d (4f) orbitals in 2p (3d) excited configurations and its effect on the x-ray and electron spectra. Tartu, 1999.

32. **Valter Zazubovich.** Local relaxation in incommensurate and glassy solids studied by Spectral Hole Burning. Tartu, 1999.

33. **Indrek Reimand.** Picosecond dynamics of optical excitations in GaAs and other excitonic systems. Tartu, 2000.

34. **Vladimir Babin.** Spectroscopy of exciton states in some halide macro- and nanocrystals. Tartu, 2001.

35. **Toomas Plank.** Positive corona at combined DC and AC voltage. Tartu, 2001.

36. **Kristjan Leiger.** Pressure-induced effects in inhomogeneous spectra of doped solids. Tartu, 2002.

37. **Helle Kaasik.** Nonperturbative theory of multiphonon vibrational relaxation and nonradiative transitions. Tartu, 2002.

38. **Tõnu Laas.** Propagation of waves in curved spacetimes. Tartu, 2002.

39. **Rünno Lõhmus.** Application of novel hybrid methods in SPM studies of nanostructural materials. Tartu, 2002.

40. **Kaido Reivelt.** Optical implementation of propagation-invariant pulsed free-space wave fields. Tartu, 2003.

41. **Heiki Kasemägi.** The effect of nanoparticle additives on lithium-ion mobility in a polymer electrolyte. Tartu, 2003.

42. **Villu Repän.** Low current mode of negative corona. Tartu, 2004.

43. **Алексей Котлов.** Оксианионные диэлектрические кристаллы: зонная структура и электронные возбуждения. Tartu, 2004.

44. **Jaak Talts.** Continuous non-invasive blood pressure measurement: comparative and methodological studies of the differential servo-oscillometric method. Tartu, 2004.

45. **Margus Saal.** Studies of pre-big bang and braneworld cosmology. Tartu, 2004.

46. **Eduard Gerškevitš.** Dose to bone marrow and leukaemia risk in external beam radiotherapy of prostate cancer. Tartu, 2005.
47. **Sergey Shchemelyov.** Sum-frequency generation and multiphoton ionization in xenon under excitation by conical laser beams. Tartu, 2006.
48. **Valter Kiisk.** Optical investigation of metal-oxide thin films. Tartu, 2006.
49. **Jaan Aarik.** Atomic layer deposition of titanium, zirconium and hafnium dioxides: growth mechanisms and properties of thin films. Tartu, 2007.
50. **Astrid Rekker.** Colored-noise-controlled anomalous transport and phase transitions in complex systems. Tartu, 2007.
51. **Andres Punning.** Electromechanical characterization of ionic polymer-metal composite sensing actuators. Tartu, 2007.
52. **Indrek Jõgi.** Conduction mechanisms in thin atomic layer deposited films containing TiO_2. Tartu, 2007.
53. **Aleksei Krasnikov.** Luminescence and defects creation processes in lead tungstate crystals. Tartu, 2007.
54. **Küllike Rägo.** Superconducting properties of MgB_2 in a scenario with intra- and interband pairing channels. Tartu, 2008.
55. **Els Heinsalu.** Normal and anomalously slow diffusion under external fields. Tartu, 2008.
56. **Kuno Kooser.** Soft x-ray induced radiative and nonradiative core-hole decay processes in thin films and solids. Tartu, 2008.
57. **Vadim Boltrushko.** Theory of vibronic transitions with strong nonlinear vibronic interaction in solids. Tartu, 2008.
58. **Andi Hektor.** Neutrino Physics beyond the Standard Model. Tartu, 2008.
59. **Raavo Josepson.** Photoinduced field-assisted electron emission into gases. Tartu, 2008.
60. **Martti Pärs.** Study of spontaneous and photoinduced processes in molecular solids using high-resolution optical spectroscopy. Tartu, 2008.
61. **Kristjan Kannike.** Implications of neutrino masses. Tartu, 2008.
62. **Vigen Issahhanjan.** Hole and interstitial centres in radiation-resistant MgO single crystals. Tartu, 2008.
63. **Veera Krasnenko.** Computational modeling of fluorescent proteins. Tartu, 2008.
64. **Mait Müntel.** Detection of doubly charged higgs boson in the CMS detector. Tartu, 2008.
65. **Kalle Kepler.** Optimisation of patient doses and image quality in diagnostic radiology. Tartu, 2009.
66. **Jüri Raud.** Study of negative glow and positive column regions of capillary HF discharge. Tartu, 2009.
67. **Sven Lange.** Spectroscopic and phase-stabilisation properties of pure and rare-earth ions activated ZrO_2 and HfO_2. Tartu, 2010.
68. **Aarne Kasikov.** Optical characterization of inhomogeneous thin films. Tartu, 2010.

69. **Heli Valtna-Lukner.** Superluminally propagating localized optical pulses. Tartu, 2010.

70. **Artjom Vargunin.** Stochastic and deterministic features of ordering in the systems with a phase transition. Tartu, 2010.

71. **Hannes Liivat.** Probing new physics in e+e− annihilations into heavy particles via spin orientation effects. Tartu, 2010.

72. **Tanel Mullari.** On the second order relativistic deviation equation and its applications. Tartu, 2010.

73. **Aleksandr Lissovski.** Pulsed high-pressure discharge in argon: spectroscopic diagnostics, modeling and development. Tartu, 2010.

74. **Aile Tamm.** Atomic layer deposition of high-permittivity insulators from cyclopentadienyl-based precursors. Tartu, 2010.

75. **Janek Uin.** Electrical separation for generating standard aerosols in a wide particle size range. Tartu, 2011.

76. **Svetlana Ganina.** Hajusandmetega ülesanded kui üks võimalus füüsika-õppe efektiivsuse tõstmiseks. Tartu, 2011

77. **Joel Kuusk.** Measurement of top-of-canopy spectral reflectance of forests for developing vegetation radiative transfer models. Tartu, 2011.

78. **Raul Rammula**. Atomic layer deposition of HfO_2 – nucleation, growth and structure development of thin films. Tartu, 2011.

79. **Сергей Наконечный.** Исследование электронно-дырочных и интерстициал-вакансионных процессов в монокристаллах MgO и LiF методами термоактивационной спектроскопии. Тарту, 2011.

80. **Niina Voropajeva.** Elementary excitations near the boundary of a strongly correlated crystal. Tartu, 2011.

81. **Martin Timusk.** Development and characterization of hybrid electro-optical materials. Tartu, 2012, 106 p.

82. **Merle Lust.** Assessment of dose components to Estonian population. Tartu, 2012, 84 p.

83. **Karl Kruusamäe.** Deformation-dependent electrode impedance of ionic electromechanically active polymers. Tartu, 2012, 128 p.

84. **Liis Rebane.** Measurement of the $W \to \tau\nu$ cross section and a search for a doubly charged Higgs boson decaying to τ-leptons with the CMS detector. Tartu, 2012, 156 p.

85. **Jevgeni Šablonin.** Processes of structural defect creation in pure and doped MgO and NaCl single crystals under condition of low or super high density of electronic excitations. Tartu, 2013, 145 p.

86. **Riho Vendt**. Combined method for establishment and dissemination of the international temperature scale. Tartu, 2013, 108 p.

87. **Peeter Piksarv.** Spatiotemporal characterization of diffractive and non-diffractive light pulses. Tartu, 2013, 156 p.